JPL Publication 82-101

DOE/ET-20356-7
Distribution Category UC-63

Cloud Cover Estimation

Use of GOES Imagery in Development of Cloud Cover Data Base for Insolation Assessment

James R. Huning
Thomas L. Logan
Jeffrey H. Smith

November 30, 1982

Prepared for
U.S. Department of Energy
Through an Agreement with
National Aeronautics and Space Administration
by
Jet Propulsion Laboratory
California Institute of Technology
Pasadena, California

JPL Publication 82-101

DOE/ET-20356-7
Distribution Category UC-63

Cloud Cover Estimation

Use of GOES Imagery in Development of Cloud Cover Data Base for Insolation Assessment

James R. Huning
Thomas L. Logan
Jeffrey H. Smith

November 30, 1982

Prepared for
U.S. Department of Energy
Through an Agreement with
National Aeronautics and Space Administration
by
Jet Propulsion Laboratory
California Institute of Technology
Pasadena, California

Prepared by the Jet Propulsion Laboratory, California Institute of Technology, for the U.S. Department of Energy through an agreement with the National Aeronautics and Space Administration.

ABSTRACT

Site selection and system engineering studies of solar energy systems require high quality insolation data of several kinds, primarily direct normal and total horizontal data. The paucity of measured insolation data has been well documented. Insolation models have been used as substitutes for the absence of measured data, but a key problem has been the need for accurate and complete information regarding turbidity, precipitable water vapor, and cloud cover to input into the models. All but cloud cover display reasonably smooth temporal and spatial behavior, but cloud cover varies rapidly both in time and space, and therefore produces large fluctuations in insolation values.

It is the purpose of this study to verify the potential of using digital satellite data to establish a cloud cover data base for the United States, one that would provide detailed information on the temporal and spatial variability of cloud development. The study involves the use of four sequential days of GOES data (eighty acquisitions) over a predetermined test area, and converts those data into a computer archive of cloud cover, one that is accessible using predetermined grid cells of variable size. Key elements include: a) interfacing GOES data from the University of Wisconsin Meteorological Data Facility with the Jet Propulsion Laboratory's VICAR image processing system and IBIS geographic information system; b) creation of a registered multitemporal GOES data base; c) development of a simple normalization model to compensate for sun angle; d) creation of a variable size georeference grid that provides detailed cloud information in selected areas and summarized information in other areas; and e) development of a cloud/shadow model which details the percentage of each grid cell that is cloud and shadow covered, and the percentage of cloud or shadow opacity. In addition, comparison of model calculations of insolation with measured values at selected test sites was accomplished, as well as development of preliminary requirements for a large-scale data base of cloud cover statistics.

ACKNOWLEDGMENT

The work reported herein was performed through NASA Task Order RD-152, Amendment 309, and was sponsored by the United States Department of Energy under IAA DE-AI01-76-ET20356, Mod. A026. Although numerous individuals contributed to this publication, three persons deserve special recognition. We wish to thank Robert Yinger, Southern California Edison Company, for his timely assistance in providing us with 1980 WEST Associates insolation data, and Dr. Macgregor Reid for critically reviewing the final draft of this document. To Arlene Calvert goes special kudos for accommodating the many unreasonable demands that were placed upon her in the preparation of the manuscript.

CONTENTS

Figures

Table

SECTION 1

INTRODUCTION

Several studies, (e.g., Reynolds, et al., 1978; Gautier, 1980, 1982; Diak, et al., 1982) have determined that the GOES satellite has the level of spatial and temporal resolution required to map cloud cover and thereby estimate insolation. The GOES satellite images every half hour with an approximate spatial resolution of 0.9 km x 0.9 km in a visible band (0.52 - 0.72 microns) and approximately 4 km x 8 km resolution in a thermal infrared band (10.5 - 12.5 microns). The visible band could be used to detect clouds during all but the winter season, when an algorithm which combines the thermal IR and visible bands to differentiate clouds and snow must be applied. Model calculations combined with actual cloud cover data for a specific site should permit the synthesis of insolation versus time curves almost as accurate as those obtained from calibrated and well-maintained instrumentation.

A fundamental issue in the assessment of the insolation resource for use in the design and evaluation of solar energy conversion systems has been the lack of a complete user requirements analysis for insolation data. Historical measurements of insolation were made to assist in agroclimatic studies, which did not require highly accurate data or frequent measurements. Monthly averages of total horizontal insolation were sufficient. Later, meteorology required data on total horizontal, direct and diffuse insolation, and the measurement frequency increased to hourly intervals. A large and diverse data bank of variable quality has resulted. These data have satisfactorily met the requirements of non-focusing or water heating solar thermal collectors, a technology that has seen renewed interest in the United States and elsewhere. Solar thermal collector technology does not require

highly sophisticated data to predict performance in a region, and the cost penalty associated with over-sizing is not prohibitive. Newer technical options that are designed to generate electricity require data of variable quality and quantity, and no single data base can suffice for an end-to-end systems analysis of those technologies. Presently, the consensus is that the most significant uncertainty is cloud cover. Existing and developing remote sensing techniques can play a major role in improving the insolation data base through assessing and mapping cloud cover, and providing those data for insolation models.

SECTION 2

BACKGROUND

Solar energy systems under design, development, and deployment at the Jet Propulsion Laboratory, California Institute of Technology, and elsewhere, require a suite of insolation data. A specific stage in the design of a system may require a level of accuracy of insolation data quite different from another stage in that same system design (Reid, et al., 1981). Once the system is deployed, data to evaluate the system performance must be taken concurrent with system operation. For example, certification of solar photovoltaic panel output performance requires very accurate measurements of insolation taken at one minute, or more frequent intervals at or near solar noon under clear skies and under specific assumptions about air mass and spectrum characteristics. In contrast to those detailed measurements, generic and initial system development activities can generally tolerate data considered to be within an accuracy level of plus or minus ten percent, at least when evaluated on an average annual basis.

Different stages of development for flat plate photovoltaics differ significantly from those of a point-focusing dish. The former uses direct and diffuse insolation and can operate at reduced efficiency even under overcast conditions, while the latter can only utilize the direct insolation and, as a function of specific system design, will not operate unless a certain minimum level of insolation is received. The higher the concentration ratio required of a system, the greater the level of measurement accuracy required to evaluate system performance. To date, SOLMET (historical measured data from 26 sites in the United States), ERSATZ (estimated data), or Typical Meteorological Year (TMY) data have been used in many programs sponsored by the U.S.

Department of Energy (DOE), although specific measurements programs at different institutions also enter into system design. Regardless of the quality of these data bases, they cannot satisfy all systems or user requirements. To a large degree, because SOLMET and TMY data are readily available, they represent the best data, and because of budgetary constraints, expansion or upgrading of the national radiation monitoring network is an uncertainty.

Evaluation of the market penetrability of a utility grid-connected solar energy system in a region depends, in large part, on the value of the electrical energy produced by that system. Although this cost is determined by a variety of factors, a major one is the match between peak output of the system and peak load demand of the utility. If the solar energy system has maximum output during peak load times, then its value to the utility or the consumer is also at a maximum. Regional variations in peak load demand, fuel mixes, and weather and climate factors will determine the viability of a solar energy option in a particular region. Several scenarios indicate that it is preferable to orient grid-connected photovoltaic systems to the southwest rather than to the south, and to locate peaking systems in areas that have a minimum of late afternoon cloud development (seasonally or annually). Clear skies in the afternoon, especially in the later hours, will allow the solar energy technology to generate the highest value of electrical energy, even though the system may not operate as efficiently as it would at solar noon. Solar system energy output may be reduced in the afternoon, but often a much better match between peak demand and system output exists at that time. Ramifications of peak load matching bear directly upon policy decisions in terms of future peaking plant construction and PURPA (Public Utility

Regulatory Policies Act of 1978) regulatory directives that both affect the utility and the consumer.

Several system performance models have been developed at JPL to assess the performance and cost of energy output for photovoltaic and point-focusing solar thermal options. These models indicate that there is a one-to-one correspondence between insolation variation and life cycle cost of energy output. If the insolation resource is underestimated by ten percent at a site then the cost of the energy output will be on the order of ten percent more than predicted. In fact, for stand-alone systems, the cost of energy output will increase by more than ten percent. Whether or not the solar energy system has storage capability affects the significance of the uncertainty in the insolation resource. Storage can smooth transients (e.g., Randall, et al., 1980) in insolation reception, but initial experiments are not planned to have storage because it adversely affects total system cost.

Because the major attenuator of insolation is cloud cover, assessment of its temporal and spatial preferences hourly, diurnally, seasonally, and annually, will resolve many site- and region-specific issues. Satellite platforms are the only means by which the assessments may be performed satisfactorily and cost-effectively. As recently reported (Stigter, 1982), the inaccuracy in relating average point cloudiness data with solar energy flux density is well documented, and Stigter suggests a method by which this inaccuracy may be avoided.

Studies by numerous investigators have shown that satellite data (GOES, NOAA) can successfully predict insolation values or be used to map cloud cover on a mesoscale and microscale (e.g., Hiser and Senn, 1980; Vonder Harr and Ellis, 1978). These studies, and others, (e.g., Hiser, 1978), have examined the relationships between total horizontal radiation measured at a

point on the ground and clouds as detected by satellite platforms sensing in the visible and thermal infrared spectra. The temporal and spatial preferences of cloud cover can be mapped at a resolution (e.g., 1 km) not previously possible with ground-based data. For large regions, or for the nation as a whole, the amount of data to be analyzed and subsequently mapped is enormous, and data management becomes the major constraint.

To extrapolate the relationship between nodal ground-based measurements of insolation data and satellite data on cloud cover to large areas requires detailed data on such parameters as air quality (turbidity), relative humidity, pressure, and ambient temperature. Fortunately, many of these data are more readily available than are data on insolation components.

A number of ramifications of these and similar studies are directly applicable to the siting of solar energy conversion systems, large central station facilities, or small dispersed systems. The most important of these is that under clear skies the amount of direct normal radiation received at the ground is nearly the same everywhere. The major differences between areas is the amount of time skies are clear, a geographic variable. Clearly, for solar thermal applications, if cloud transients or cloud cover can be mapped and statistical probabilities developed for sites or homogeneous regions to predict the development and persistence of cloud in an area, a major uncertainty in the viability of solar energy systems could be resolved. These analyses can affect such factors as facility sizing, orientation, and storage capacity.

Simple and sophisticated models have been developed to extrapolate insolation components (Randall and Whitson, 1977) or interpolate to areas, but these models have not been sufficiently tested with high quality data from

many locations. Uncertainties arise as to their adequacy to predict or assess insolation resources in areas selected for solar energy system deployment.

Those general remarks have been summarized by Hulstrom of the Solar Energy Research Institute. Hulstrom canvassed the solar energy community on user requirements for insolation data on a mesoscale (i.e., 100 km x 100 km), and determined that several options could be taken to meet stated requirements of the solar energy community (Hulstrom, 1981). These options include:

(1) the establishment of a dense insolation measurement network over the United States;

(2) derivation of suitable site-to-site interpolation techniques so that the existing SOLMET/ERSATZ data base could be used to develop an insolation data base;

(3) utilization of satellite (GOES) platforms to map cloud cover/ insolation variations, and,

(4) combining all of the above to develop the most meaningful insolation data base.

Each option has certain advantages and disadvantages associated with it, but basically the establishment of a dense measurement network would require on the order of 1,000 stations, assuming a spacing of approximately 100km. To establish these stations would require an investment of approximately five million dollars just for instrument and hardware acquisition. The associated maintenance, data collection and data archiving would cost approximately three million dollars per year. Both estimates are considered conservative, and the actual costs could be more than twice those estimates. The network would be established to provide hourly direct and global insolation values.

The second option, development of suitable interpolation routines, has too much uncertainty associated with it. If sufficient small-scale

insolation data were available to develop an adequate interpolation technique, the techniques would only be applicable at the data sites since interpolation assumes homogeneity between data points. Too little is understood about regional variations and interpolation to allow reliable regional extrapolations.

The third option, that of using satellite platforms, has already been demonstrated to have high spatial resolution a temporal resolution of one-half hour, and an accuracy within approximately 10 percent (of the accepted ground based measurements, which in turn has associated errors/uncertainties. As noted, previous studies have demonstrated the utility of using satellite data to map mesoscale insolation (e.g., Vonder Haar and Ellis, 1975, 1978; Reynolds, et al., 1978; Tarpley, 1979; Gautier, et al., 1980; Gautier, 1982), but the satellite option can quickly result in a massive data handling problem.

There are several options available to reduce the volume of data that must be handled: (1) mapping could be performed at a resolution of 50 km x 50 km or possibly larger; (2) insolation could be mapped for specific areas of particular interest to the solar energy community (e.g., urban areas, coastal locations where insolation variation is high), or 3) satellite data could be used to derive applicable interpolation procedures for the SOLMET/ERSATZ and new NOAA data collection network (although the future of this network is uncertain). The primary purpose of this study is to map cloud cover at a high resolution and define a data management strategy to handle the enormous amount of data.

SECTION 3

DATA MANAGEMENT: VICAR/IBIS

Technologists concerned with the engineering of solar energy systems conclude that any resources assessment program for solar energy would require a highly sophisticated data base, with subsequent modeling of insolation behavior. Discrete temporal and spatial resolution is needed to answer basic questions relating to siting, design, sizing, and cost-effectiveness of solar energy systems. An upgraded data base should address the following questions:

(1) What is the longest period of continuous cloud cover for a site during each month? These data would provide the basic information needed for system storage design.

(2) How variable is hourly and daily insolation for different times of the day or year? This would provide engineers with data on a system's energy generation and performance potential.

(3) How significantly is insolation affected by regular cloud buildup at certain hours of the day during different seasons? This result may, for example, permit optimization of solar panel positioning.

(4) What is the actual insolation budget for an area over time? How does it differ from adjacent regions due to microclimatological affects? Such data would assist in the optimal positioning of large installations by utility companies.

Rarely can these questions be addressed by meteorological station data because of the dual requirement for several years of data collection and a spatially dense network of readings. As noted, previous studies have shown that it is possible to use GOES data to compute insolation. Furthermore, GOES can

provide the spatial and temporal resolution required to achieve an understanding of the occurrence of mesoscale variations in insolation (Hay, 1980). Furthermore, cloud and sky cover are usually visual measurements of a qualitative nature. Remote sensing of cloud cover could significantly improve the quantitative usefulness of these variables for models and other applications. This capability is achieved only with a tremendous burden in data volume* and the technical challenge to efficiently convert image rasters to tabular and graphical files. The general purpose IBIS geographic information system technology and associated VICAR image processing system developed at JPL's Image Processing Laboratory provides one form of technology capable of handling the large volumes of data involved.

Only the salient features of VICAR/IBIS are given here, but for the interested reader, Appendix I provides a comprehensive description. In essence, digital image processing utilizes the basic premise that geocoded data sets can be referenced to a raster scan, which is basically an ultrafine grid cell mesh data set. One advantage of this format is that geographical locations or points can be accessed rapidly by their positions in the image matrix. Many data types and data sources, when converted to the image format, provide a series of data planes that can be overlaid in any combination desired by the user and then analyzed. Output products can range from images and maps to tabular printouts as a function of user needs. Thus, large amounts of data can be analyzed and manipulated to user specifications, which is a primary requirement of this study.

---

* For a nominal three year cloud cover data base of the continental United States, with an average of 24 half hourly acquisitions, some one billion bits must be registered, interpreted, and converted to tabular files each day. This converts to approximately 1×10^{12} bits for a 3 year period.

SECTION 4

STUDY AREA

A. INTRODUCTION

The large amount of data an operational system would require, and the capability to analyze and display that data would overwhelm many software-hardware configurations. For the current study, only four days of half-hourly GOES imagery were used, and for technical reasons, only the visible channel was used in the research. The specific test area was selected because it represented a wide variety of physiographic and climatic types. Perhaps even more importantly, a dense network of insolation measuring stations is located within the test area (WEST Associates), and therefore provided high quality ground truth with a high frequency of temporal and spatial resolution for this and subsequent analyses. The test site includes much of southern California, as well as small portions of western Arizona and southern Nevada. The entire test area covers approximately one-sixtieth of the continental United States.

The test site was regionalized into a number of generally homogeneous climatic and physiographic units. The primary purpose of the regionalization was to determine how significantly computational time could be reduced without loss of accuracy as compared to the cost of analyzing individual pixels--the concept of a variable grid size was used. Not only was computational time reduced, but also output information was reduced to a manageable level. Aggregated grid cell size ranged from 3.6 km x 3.6 km in the coastal and urban areas to 28.8 km x 28.8 km in western Mojave, an area characterized by nearly level terrain. The western Mojave is generally isolated from the influence of unstable maritime tropical (mT) air masses that advect either

from the Gulf of California (surface flow) or the Gulf of Mexico (anticyclonic circulation). During summer and fall seasons these air masses can produce significant cloud cover and precipitation over the Salton Trough and eastern Mojave, as well as places farther east. The regionalization process also allows for an evaluation of the efficiency of regional extrapolation of insolation for the test area from specific sites where insolation was measured.

B. REGION DESCRIPTIONS

The selected regional breakdown is given in Figure 4-1. Twenty specific regions were used in the analysis to generate cloud cover statistics on a variable size grid basis. Descriptions of the twenty subregions follow.

REGION	SYMBOL	AREA (km^2)	DESCRIPTION
1	EMJ1	41,522	EMJ1 defines much of the eastern Mojave, i.e., the area west of Barstow. The area is characterized by considerable local relief.
2	MTN3	3,120	MTN3 is a highland area within the EMJ1 region; it was separated from EMJ1 because of its orographic effect on advecting air masses.
3	MTN1	962	MTN1 is in the extreme northwest corner of the study area; it includes the southeast portion of the Tehachapi Mountains. MTN1 receives more cloud cover and precipitation than does the western Mojave unit.
4	WMJ1	14,170	WMJ1 represents most of the western Mojave, and it contrasts with the eastern Mojave by its more level terrain. WMJ1 is also isolated from advecting mT air because of the Transverse Ranges.

ORIGINAL PAGE
BLACK AND WHITE PHOTOGRAPH

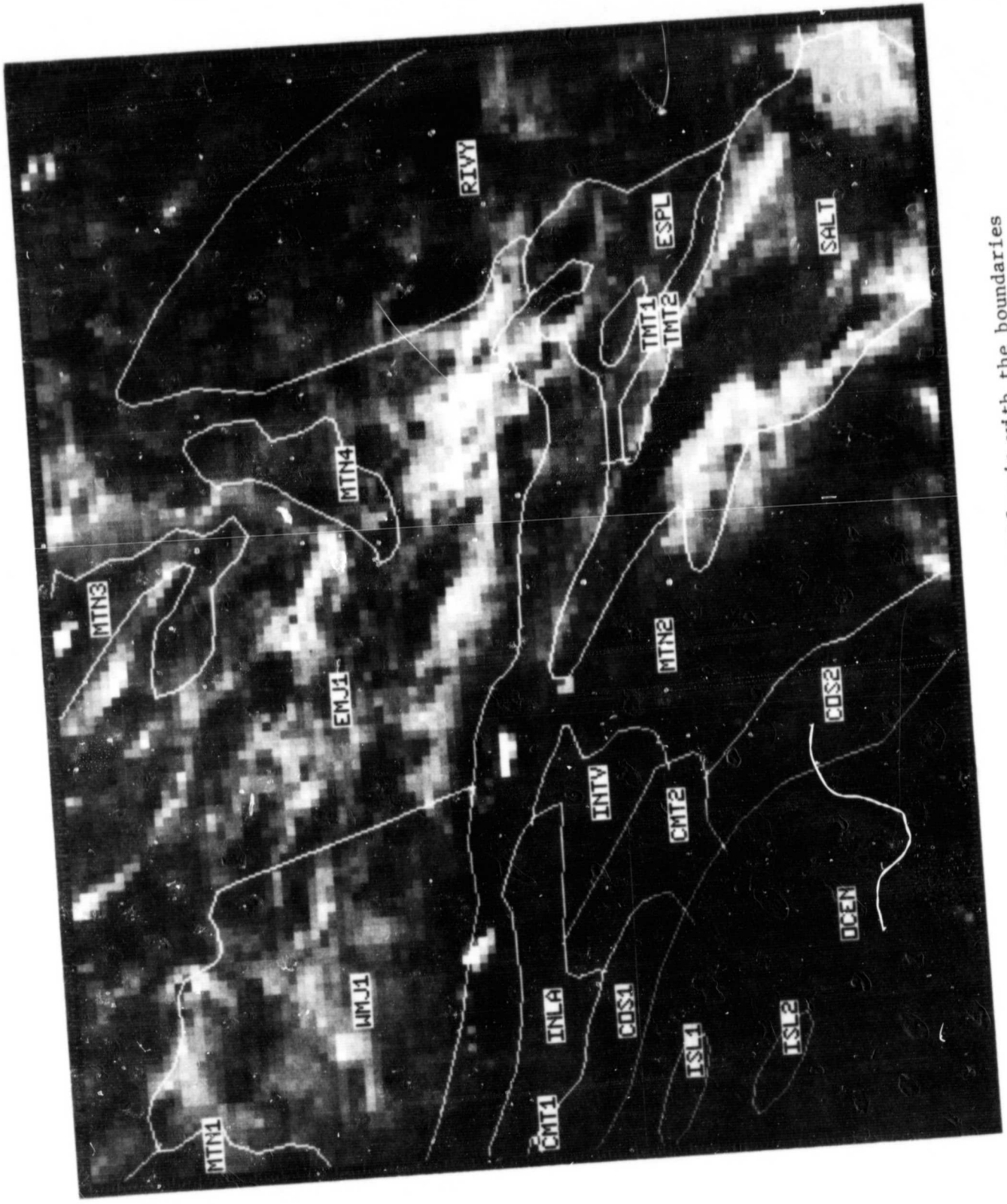

Figure 4-1. GOES image of southern California with the boundaries of the 20 physiographic/climatic regions superimposed.

REGION	SYMBOL	AREA (km^2)	DESCRIPTION
5	RIVY	10,582	RIVY comprises a large portion of the area of the Colorado River Valley. It regularly (but infrequently) has afternoon cloud cover and/or thunderstorm activity during late summer and early fall.
6	MTN4	2,288	MTN4 is a small area located within the Eastern Mojave. It was broken out because of the "trigger" effect it may have on advecting mT air masses.
7	MTN2	18,473	MTN2 represents a small area bordering the Salton Trough that impedes air flow from the south.
8	INLA	3,172	INLA consists of the area inland of the coast and borders the Transverse Ranges. It is characterized by urbanization.
9	CMT1	39	CMT1 is a very small area of hilly terrain on the western edge of the study area.
10	COS1	2,288	COS1 represents the coastal fringe of Long Beach/Los Angeles/Orange County. It is heavily urbanized and has a high degree of cloud cover variability.
11	INTV	2,132	INTV is the interior valley and is also heavily urbanized, but it is isolated from direct coastal influence by CMT2.
12	CMT2	2,535	CMT2 is similar to CMT1, and includes the coastal mountains of Orange County.
13	OCEN	10,075	OCEN is all the ocean area, excluding two islands.
14	SALT	9,100	SALT refers to the Salton Trough, primarily comprising the Imperial and Coachela Valleys.

REGION	SYMBOL	AREA (km^2)	DESCRIPTION
15	ESPL	3,146	ESPL defines the area between the Salton Trough and the Colorado River Valley.
16	TMT1	312	TMT1 is a small area within the ESPL. It was separated out because of likely orographic effects these mountains should have on mT air masses.
17	ISL1	754	ISL1 is Santa Catalina Island.
18	TMT2	858	TMT2 is similar to TMT1, and it separates SALT from ESPL.
19	COS2	2,223	COS2 is similar to COS1, but it is located south of the coastal mountains in Orange County. It includes the urbanized area in and near coastal San Diego.
20	ISL2	949	ISL2 is San Clemente Island.
	Total Area = 128,700 km^2		

SECTION 5

INSOLATION DATA

For estimation of insolation data using existing models and cloud statistics generated from this study, and to assist in model evaluation, high quality ground-based measurements of insolation were required. One reason for selecting the southern California area was that many insolation measuring stations maintained by the WEST (Western Energy Supply and Transmission) Associates are located in it. WEST Associates is a consortium of utilities that operate in the Western United States (Yinger, 1982).

WEST Associates funds the Southern California Edison Company for project management of the insolation program, which includes instrument calibration, data translation and storage, data reduction, and generation of annual reports. Each cooperating utility provides the monitoring equipment, station set-up costs, maintenance, data tape changes, and an adequate site.

In 1981 a total of 51 stations comprised the network. Every station monitors and records total horizontal insolation and dry bulb temperature. Total insolation is measured by one of three pyranometers: Eppley Black and White; Eppley Precision Spectral, or the Spectrolab Spectrosun SR-75. In 1980, 26 stations also monitored direct normal insolation using an Eppley Normal Incidence Pyrheliometer (NIP).

To insure the highest degree of consistency and accuracy possible, the WEST network follows a rigorous maintenance and calibration program. Maintenance is performed weekly at all stations that record total insolation and dry bulb temperature, and three times per week at stations that also monitor direct normal insolation. The Southern California Edison Company calibrates all instruments on an annual basis. The Eppley NIPs are calibrated

with a Kendall Mark VI cavity radiometer. Pyranometers are calibrated with standard pyranometers, which in turn are calibrated by the sun and shade method with a standard pyrheliometer or cavity radiometer.

Data tapes from each station are changed once per month, and the tapes are read and translated at Southern California Edison's main facility in Alhambra, California. The final data base consists of insolation and temperature values averaged over 15 minutes for the entire year. Some data are lost during the year, but typically the majority of these losses occur at only a few stations; data losses are small for the majority of stations. Very few losses occurred from the 21 stations in the network maintained by Southern California Edison, which maintains nearly all of the monitoring stations within our specific test area. The primary reference station used in this study, Alhambra, California had no missing total horizontal data, while Barstow and Blythe lost one percent (none was lost during April). More direct normal insolation data were missing than total horizontal, but none for the four day period of our study.

Effective this year, 1982, the network ceased to exist as a unit. Each utility will be responsible for calibrating their own instruments, and each will be responsible for any data reduction or reporting of data.

SECTION 6

DATA PROCESSING FOR CLOUD STATISTICS

A. ARCHIVED SATELLITE DATA

GOES data used in the test study were obtained from the Space Science and Engineering Center (SSEC) archive at the University of Wisconsin. Data were provided to JPL in a two-dimensional format with 8-bit pixels and a single tape header record. SSEC refers to this as "SAVE-TAPE" format. A VICAR program named "VGOES" was written to reformat the 24-bit word size of the SSEC data to IBM 32-bit word size and separate individual images. All eighty images of the study area are shown on Figure 6-1.

To optimally conduct the cloud cover modelling project, the raw GOES data needed to be arranged sequentially by time and date, as separate image files. Arranging the University of Wisconsin data to this specification proved difficult for the following reasons:

(1) Fifteen images were arranged back-to-back with no file headers or end-of-file marks on each tape. To extract an image from a tape required processing all preceeding images on that tape.

(2) Single GOES visual images were stored on tape in left and right halves (each 2320 lines by 1008 samples), requiring the two files to be merged for study areas straddling the artificial division. The thermal infrared data (580 lines by 1008 samples) were not similarly divided.

The SSEC format also resulted in difficulties when a rare JPL tape drive malfunction resulted in the physical stretching of one of the GOES thermal infrared (TIR) tapes. Since the location of each image is only known relative to the beginning of each tape, the starting position of all images

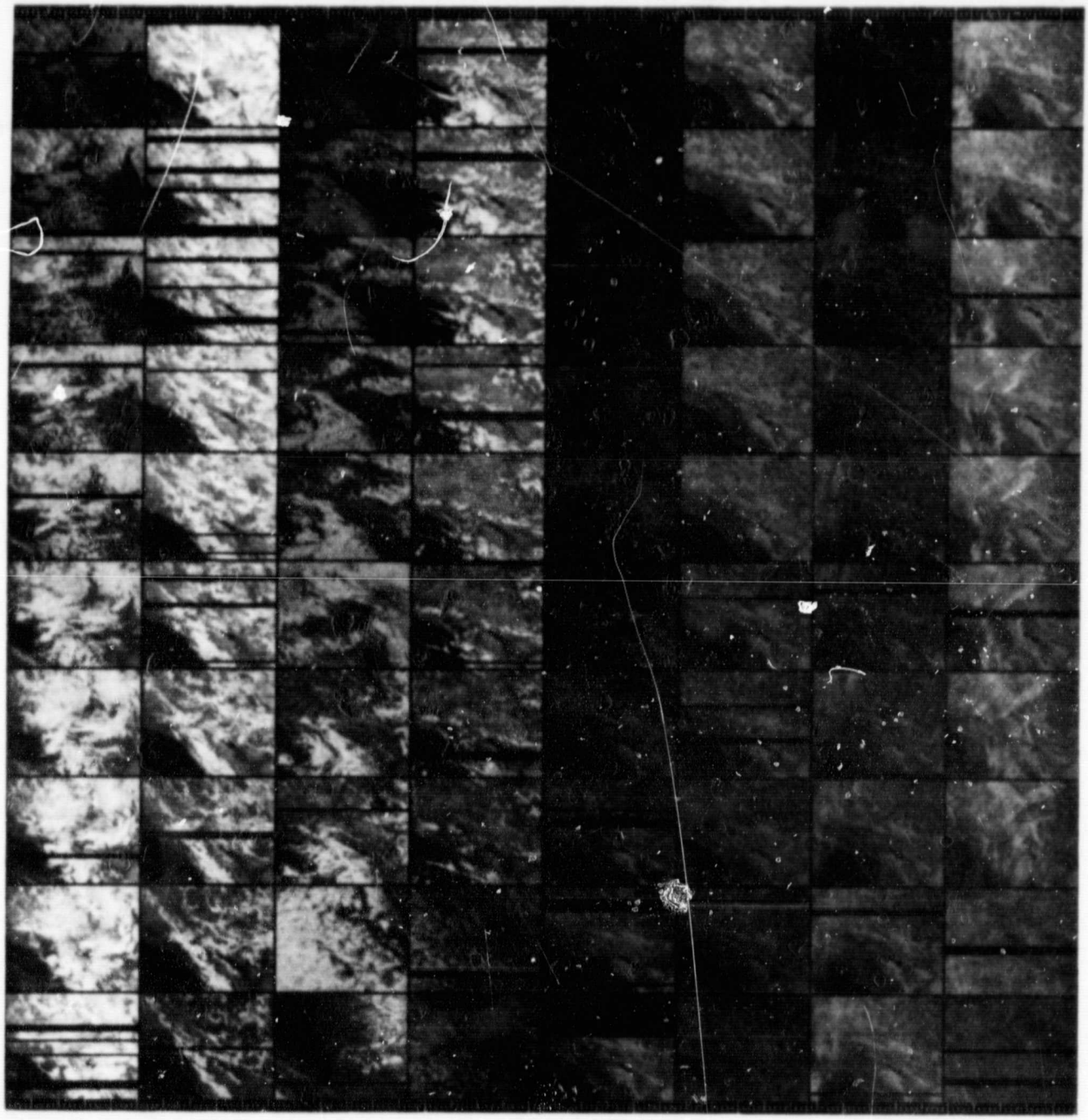

Figure 6-1. Reduced images of all 80 acquisitions. For each day 20 images were required. Acquisitions for each day are presented in two columns. The first acquisition on 1 April 1980 (1415 GMT) is at the upper left, while the last acquisition on that day is the last image in column 2. Likewise, the 20 images analyzed for 2 April consist of images in columns 3 and 4.

past the stretch zone were changed and had to be individually located. Because of time constraints, this work could not be done, and TIR data were dropped from the analysis. The primary value of TIR data is to allow the differentiation of snow from cloud, although assessments of atmospheric moisture are also possible. As the test area possessed no significant amount of snow during the four day study period, non-use of the TIR data did not significantly impact the course of the research.

B. DATA QUALITY

A large proportion of dropped or missing data was detected in the SSEC GOES VS and TIR imagery. This manifested as all black, all white, or garbled lines, often occurring in large blocks (Figures 6-2 and 6-3). Where drops occurred, there was generally too much missing data to repair. Typically, the simplest procedure to repair data drops involves interpolating from the nearest good data. However, to follow this procedure given the large area of data drops, would have produced biased cloud cover inventory results.

Garbled data were similarly difficult to repair. The problem with garbled data is that its historgram often appears similar to a histogram of good data. Should a technique that removes potentially garbled data be used, unreliable analysis might result because the technique would likely miss bad data and repair good data. The general quality of the SSEC supplied data was good, although there appeared to be a sensor banding problem. Removal of the banding would not be difficult, although it would be time consuming.

Based on the completed pilot study, it is not recommended that the archived data available from the SSEC of the University of Wisconsin be used for developing a cloud cover data base for the United States. It is probable

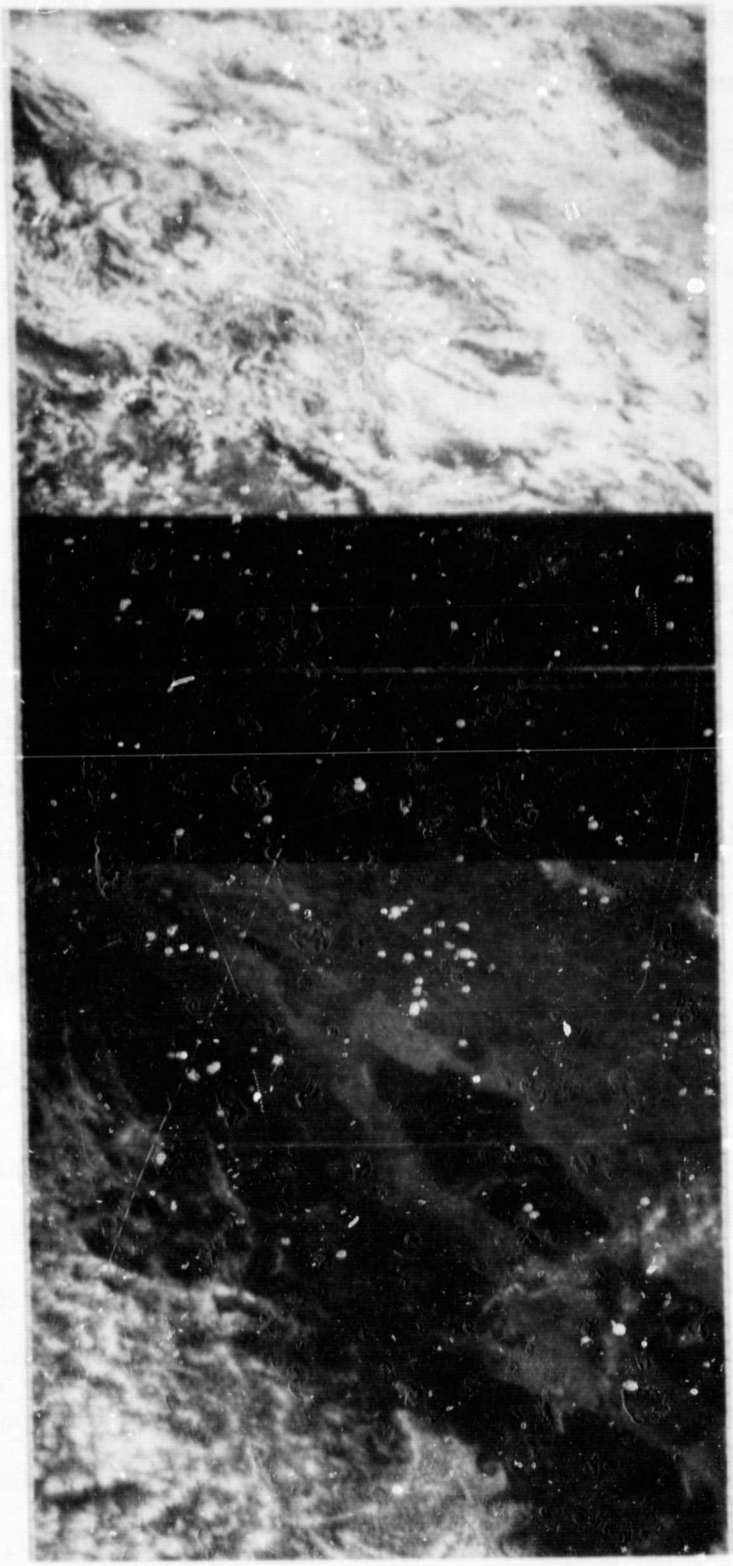

Figure 6-2. For a number of images a significant amount of data are missing, such as the large data void in the central portion of this image (3 April 1980).

Figure 6-3. Missing and garbled data on a typical thermal infrared image.

that too much time would be required to process the data into a usable format, with subsequent costs likely to become large.

C. IMAGE REGISTRATION

The supplied GOES data registration offsets proved insufficient for the accurate frame-to-frame registration necessary for this research. All offsets and registration were performed with 0.9 km x 0.9 km data. To determine initial offset estimates for the southern California study area, the following formulae were used:

VS OFFSET:

Lines: (1870-(Origin Starting Line))+1100

Samples: 9546-(Origin Starting Sample)

Once general registration offsets were calculated, a VICAR/IBIS procedure was developed to register each frame individually. The heart of the procedure is the PICMATCH program. PICMATCH uses Fast Fourier Transform (FFT) Phase to correlate selected Ground Control Points (GCPs). For this test study, a master frame was selected and all frames were registered to it. The master frame represents the best cloud-free image of the eighty frame sample. Twenty GCPs were selected from throughout the study area image for registration. Twenty GCPs are more than are necessary for a test area the size of southern California, but that number was used to determine the cost of registering a complete GOES frame. Approximately one minute of computer CPU time (IBM 370/158) per image was found to be sufficient for the task. GCP offsets were determined relative to the master frame and subjected to the following hierarchical editing scheme:

(1) All GCPs that had an FFT Phase correlation value below 130 (out of 950 maximum) were removed. Correlations below 130 were regularly found to be incorrect.

(2) All GCPs that had a DN value difference between the master and selected frame of more than 100 were removed. This removed all GCPs that were erroneously correlated on clouds or shadow.

(3) If six or more GCPs remained, a regression was performed on the GCP's line and sample coordinates (should fewer than six GCPs remain, steps 4 and 5 are followed). Any GCP that had a regression residual less than -3 or greater than +3 was removed. Should three or less GCPs remain after the regression, step 3 results are ignored, and steps 4 and 5 are performed. If more than 3 GCPs remain after regression, step 4 is skipped.

(4) Remove all GCPs with a correlation below 248. No correlations above 248 were found to be incorrect.

(5) For all GCPs remaining after completing the prior steps, offset values relative to the master frame were averaged to produce the final values.

No correlations could be obtained for those frames with significant cloud cover. For those frames, the calculated offsets of all eighty frames were placed in a table and missing offsets interpolated from them.

A plot of GCP registration residuals for a selected frame are shown in Figure 6-4 and demonstrate the stable interior geometry of the GOES VS imagery. To register all images against the master, therefore, only required simple offset adjustments in the horizontal and vertical directions. A 'rubber sheeting' procedure to register the imagery was not required. However, a similar stable geometry for the TIR imagery has not been verified.

ORIGINAL PAGE IS
OF POOR QUALITY

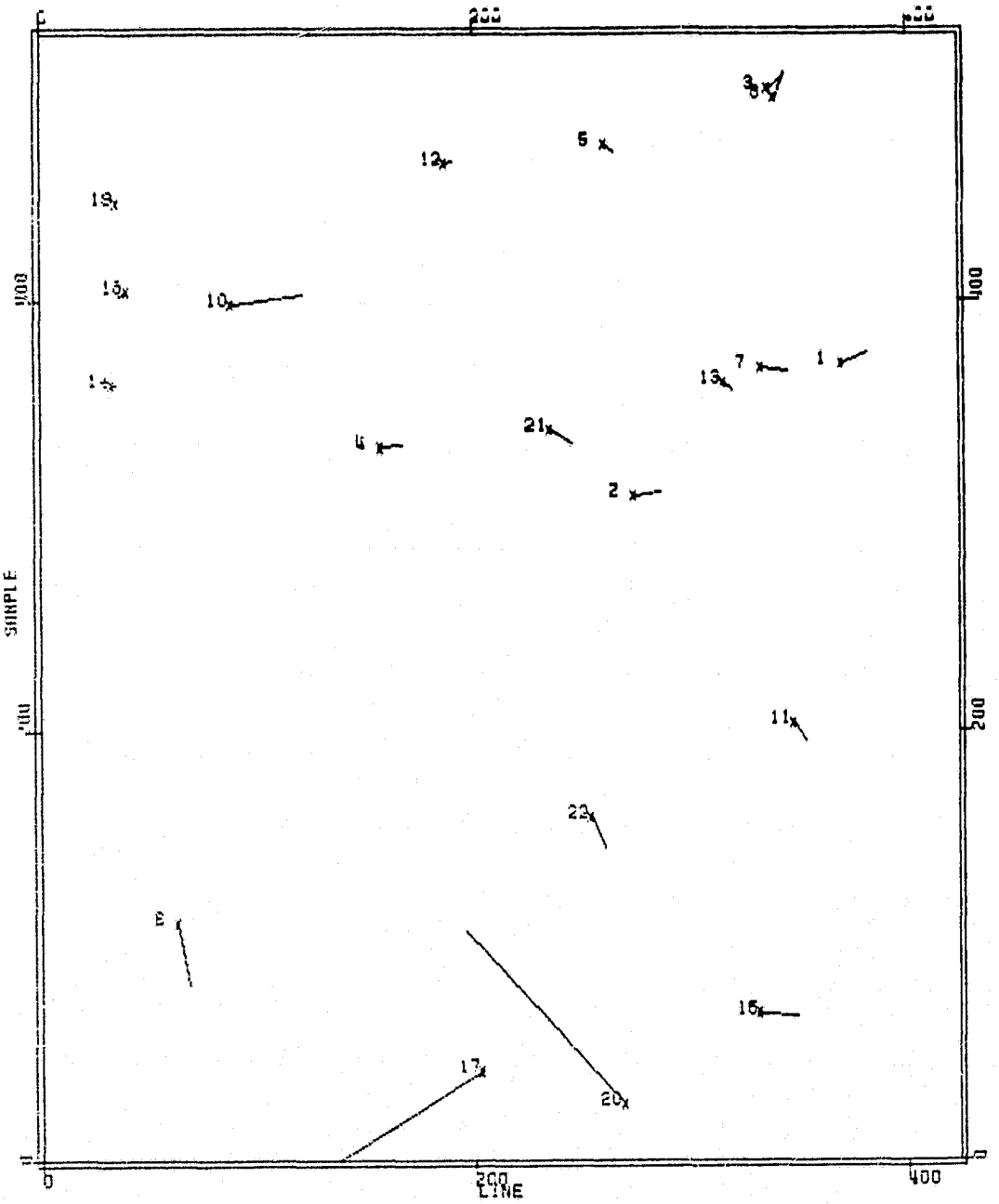

Figure 6-4. The plot represents the internal stability of the GOES platform. An 'x' or short line segment indicates that the images could be matched well from one to the next; a long line segment (10, 17, 20) indicates that cloud cover precluded an accurate match.

An indication of the degree to which line and sample offsets had to be corrected for the VS data is given by the maximum pixel shifts for the eighty frame sample. Line offsets ranged up to 36 pixels (35.1 km), and sample offsets up to 22 pixels (19.8 km). Errors of this magnitude are consistent with those reported by Sutherland et al. (1979). For five of the eighty images, offsets were entirely incorrect and resulted in the wrong areas accessed. Time constraints prevented any attempt to locate correct offsets for the five images. Clearly, the offsets provided with the archived data are insufficient for detailed analysis of the GOES imagery. The specific offsets used for the images are given in Table 6-1.

D. IMAGE NORMALIZATION

Because of earth rotation, solar reflectance and insolation values vary markedly from sunrise to sunset. Unless some technique is used to compensate for these changes, neither cloud signature nor shadow effects can be differentiated from changes in solar reflectance. The technique used in this test study is not intended to be adapted to an operational system, but it does provide a rational framework for additional evaluation and development.

A flat and clear area was chosen as the reference standard. The area covered a 3 pixel by 3 pixel site near Blythe, California (about 7.3 km^2). The 3 x 3 pixel area was extracted from the imagery, density values averaged, and plotted for one daily cycle (Figure 6-5). The plot was smoothed slightly, and difference ("normalization") values were calculated by substituting each half-hour density value from the midday's highest value (2115 GMT). The appropriate half-hourly normalization value was then subtracted from the master frame in order to approximately match the density values of all eighty frames imaged at different times of the day. This technique works satisfac-

TABLE 6-1

GOES VISUAL OFFSETS

Image	Date	GMT	Line Offset	Sample Offset	Notes
1	1 April 80	1415	3	-12	
2		1445	11	-13	
3		1515	10	-13	
4		1545	10	-14	
5		1615	9	-12	interpolated
6		1645	7	- 9	
7		1715	7	- 9	interpolated
8		1745	8	- 8	
9		1815	7	-10	interpolated
10		1845	6	-12	
11		1915	4	-13	
12		1945	2	-15	interpolated
13		2015	0	-20	
14		2045	2	- 7	
15		2115	2	- 6	
16		2145	0	- 6	
17		2215	8	- 4	
18		2245	0	- 9	
19		2315	0	- 8	
20		2345	- 8	- 6	
21	2 April 80	1415	16	- 9	
22		1445	16	- 9	
23		1515	16	-10	
24		1545	6	-11	
25		1615	6	-12	
26		1645	0	0	wrong area
27		1715	12	- 7	
28		1745	18	- 4	
29		1815	0	0	wrong area
30		1845	0	0	wrong area
31		1915	- 2	- 2	
32		1945	- 3	0	
33		2015	12	0	
34		2045	10	0	
35		2115	9	- 7	
36		2145	8	- 7	
37		2215	- 9	- 5	
38		2245	-10	- 5	
39		2315	0	0	wrong area
40		2345	0	0	wrong area

TABLE 6-1
(con't)

Image	Date	GMT	Line Offset	Sample Offset	Notes
41	3 April 80	1415	13	-12	
42		1445	20	-13	
43		1515	20	-12	
44		1545	19	-15	
45		1615	26	-10	
46		1645	9	-12	
47		1715	7	- 7	
48		1745	6	- 6	
49		1815	12	- 8	
50		1845	18	-10	
51		1915	16	-10	
52		1945	14	-10	
53		2015	4	- 8	
54		2045	2	- 1	
55		2115	0	0	master reference
56		2145	- 2	1	
57		2215	- 3	2	
58		2245	- 5	- 6	
59		2315	- 6	- 5	
60		2345	- 7	- 5	
61	4 April 80	1415	24	- 8	
62		1445	24	- 8	
63		1515	24	- 8	
64		1545	14	-11	
65		1615	21	-11	
66		1645	12	-11	
67		1715	10	- 7	
68		1745	24	- 6	
69		1815	22	- 9	
70		1845	19	- 8	
71		1915	1	- 5	
72		1945	- 2	- 5	
73		2015	4	- 2	
74		2045	1	- 2	
75		2115	7	- 6	
76		2145	5	- 5	
77		2215	- 6	- 4	
78		2245	- 7	- 2	
79		2315	- 7	0	interpolated
80		2345	- 7	0	interpolated
	Offset maximum		-10	-20	
	and minimum		26	2	
		Range	36	22	pixels

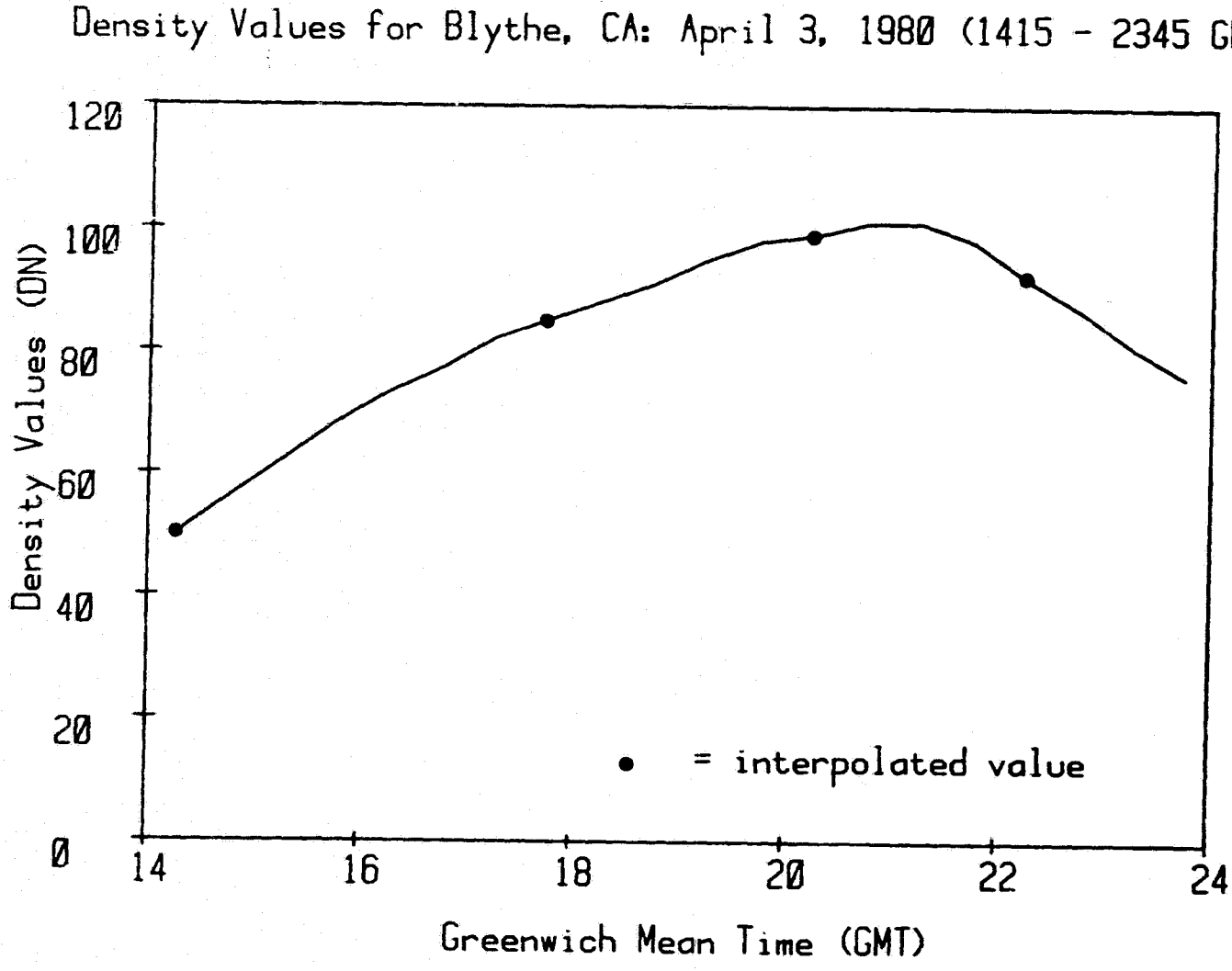

Figure 6-5. The plot represents density values for the Blythe, CA (3 April 1980) image. Because this image was the clearest one in the 80 image acquisition, it was used to generate a master reference frame for the remaining images.

torily for small study areas, but would probably not be suitable for large images where solar reflectance varies considerably from one side of the image to the other.

E. GEOREFERENCE GRID

The original GOES VS data had a pixel resolution of 0.9 km x 0.9 km. Once the registration process was complete, the VS data were degraded to 3.6 km x 3.6 km (4 x 4 pixels) to reduce the size of the data set. As previously noted in Section 4, not all areas needed to be evaluated at the smallest resolution (3.6 km x 3.6 km) so the test area was partitioned into regions of geomorphic and climatic homogeneity. Because of this regionalization, a variable grid cell size was used, with the highest resolution (smallest grid cell size) in coastal environs, or in areas where a high degree of spatial variation in cloud cover was expected. For the analysis, grid cell areas ranged from approximately 13 km^2 to 830 km^2:

(1) 3.6km x 3.6km: Coastal Margin (COS1; COS2), Islands (ISL1; ISL2).

(2) 7.2km x 7.2km: Inland (INLA), Interior Valley (INTV), Test Mountains (TMT1; TMT2).

(3) 14.4km x 14.4km: Coastal Mountains (CMT1; CMT2), Mountains (MTN1; MTN2; MTN3; MTN4), East Mojave (EMJ1).

(4) 28.8km x 28.8km: West Mojave (WMJ1), Salton Trough (SALT), Colorado River Valley (RIVY); East Salton Plain (ESPL).

The physiographic regions were coordinate digitized from a 1:500,000 U.S. Geological Survey map, and converted into image format with a unique number assigned to each region. Grid cells of the appropriate size were then assigned to cover each region (Figure 6-6) using a VICAR/IBIS procedure.

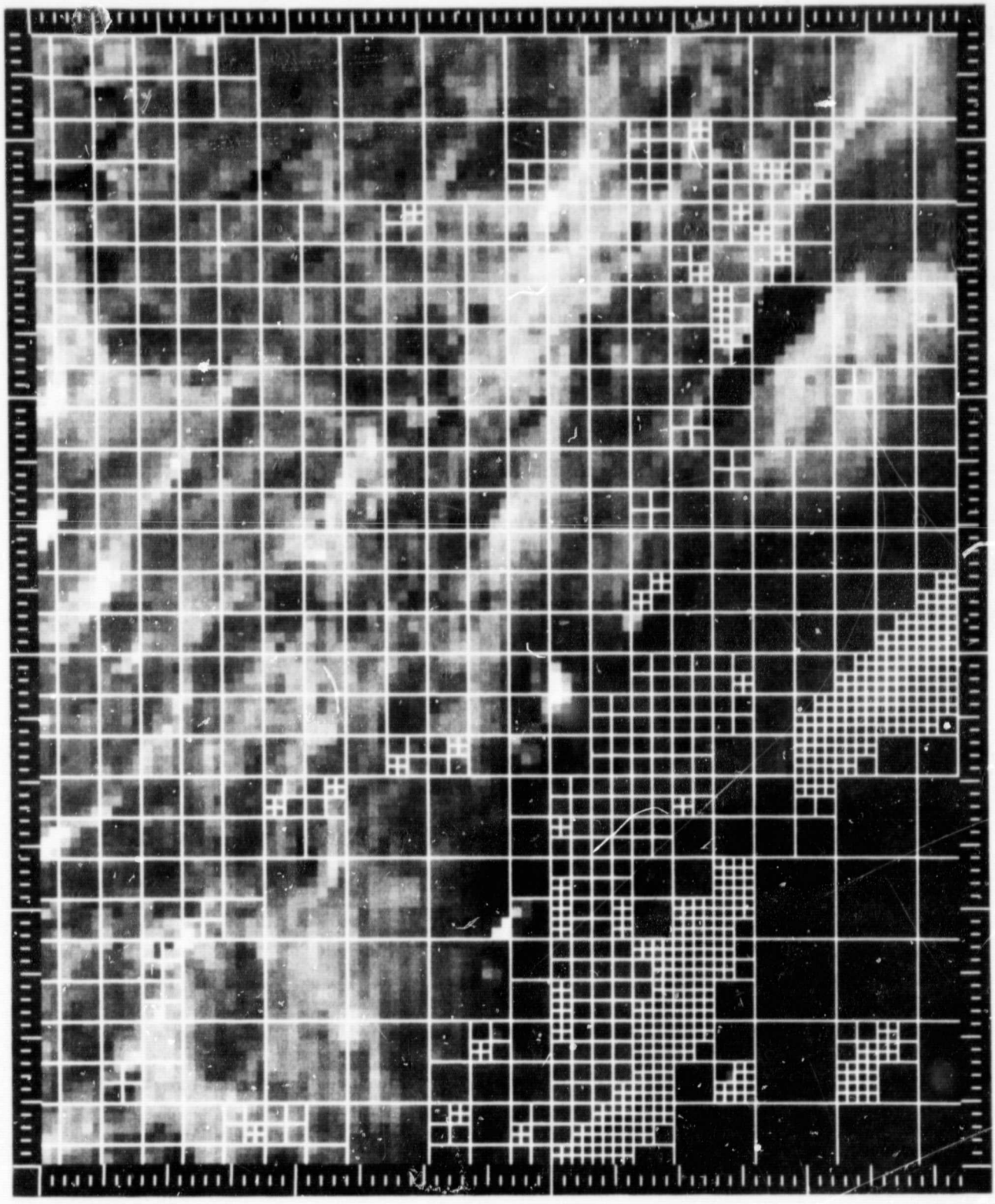

Figure 6-6. The georeference grid superimposed upon an image.

F. CLOUD/SHADOW ESTIMATION

The Image Based Information System (IBIS) was used as the primary vehicle to determine clouds, shadows and their relative opacity. The key differentiation between IBIS methodology and other technology is that all image data are converted into conceptually columnar format. Processing proceeds as row operations applied to column formatted data (Appendix 1).

The southern California study area comprised 9900 GOES VS pixels (each 3.6 km x 3.6 km) apportioned over 1247 variable sized georeference grid cells. As previously described, the square grid cells contained 1 (1 x 1 pixel), 4 (2 x 2 pixel), 16 (4 x 4 pixel), or 64 (8 x 8 pixel) VS pixels, depending on the physiographic region they represented. All processing was performed at the pixel level but aggregated and reported by georeference grid cell, except the one pixel grid cells, which could only be 100 percent cloud, 100 percent shadow, or 100 percent clear.

The basis of the cloud cover model involves differencing each of the eighty GOES frames from the cloud and haze free master frame, which is first normalized by the appropriate solar reflectance difference value. A series of IBIS functions were applied to calculate cloud, shadow, and the opacity of the cloud and shadow. All DN (density number or pixel grey tone value) differences greater than 6 were considered to represent the presence of clouds. DN differences less than -6 were considered to represent shadow. The difference threshold of '6' represents the 'noise' level that must be exceeded before a DN difference can be considered of sufficient significance to warrant classification as cloud or shadow. The value 6 was determined from the Blythe normalization test, where the maximum DN change between one-half hour daily periods was 6. The number of pixels in each georeference grid identified as cloud or shadow were then converted to a grid cell percentage and reported.

The next step was to identify all GOES pixels with DN values of less than 25. Examination of all eighty GOES VS frequency historgrams revealed that no true data values occurred that were less than 25 DN. Therefore, any value below that number represented bad data. As mentioned in Section 5.2, bad data manifested as all black, all white, or garbled DN values. The 'bad' data flagged in the final summary tabulations only reliably identifies the 'all black' and some of the garbled bad data. The 'all white' bad data could not be separated from good data on the basis of the frequency histograms. Bad data pixels were converted to a percentage of their resident grid cell and reported.

Cloud and shadow opacity percentages were estimated based on the assumption that any DN difference greater than (or less than for shadow) four times the noise level represented 100 percent opacity. Thus, any DN difference of 24 (for clouds) or -24 (for shadow) was determined to represent a 100 percent opaque situation. Because the first six DN differences were considered to represent noise, no opacity percentages below 25 percent (except for 0%) are possible in the final reported tabulations. Any DN differences greater than 24 or less than -24 were saturated to 100% opacity.

The inverse of the IBIS processing format is produced by the MAPGEN program which converts column data back into image format. A number of MAPGEN images were produced to display the results of the cloud cover mapping tabulations. Figures 6-7, 6-8, 6-9 and 6-10 show cloud coverage, shadow coverage, and their relative opacity for April 2, 1980, 1515 GMT.

G. SYSTEM DISCUSSION

Comparison of the cloud cover model results with ground based insolation measurements suggest that the model and its assumptions are

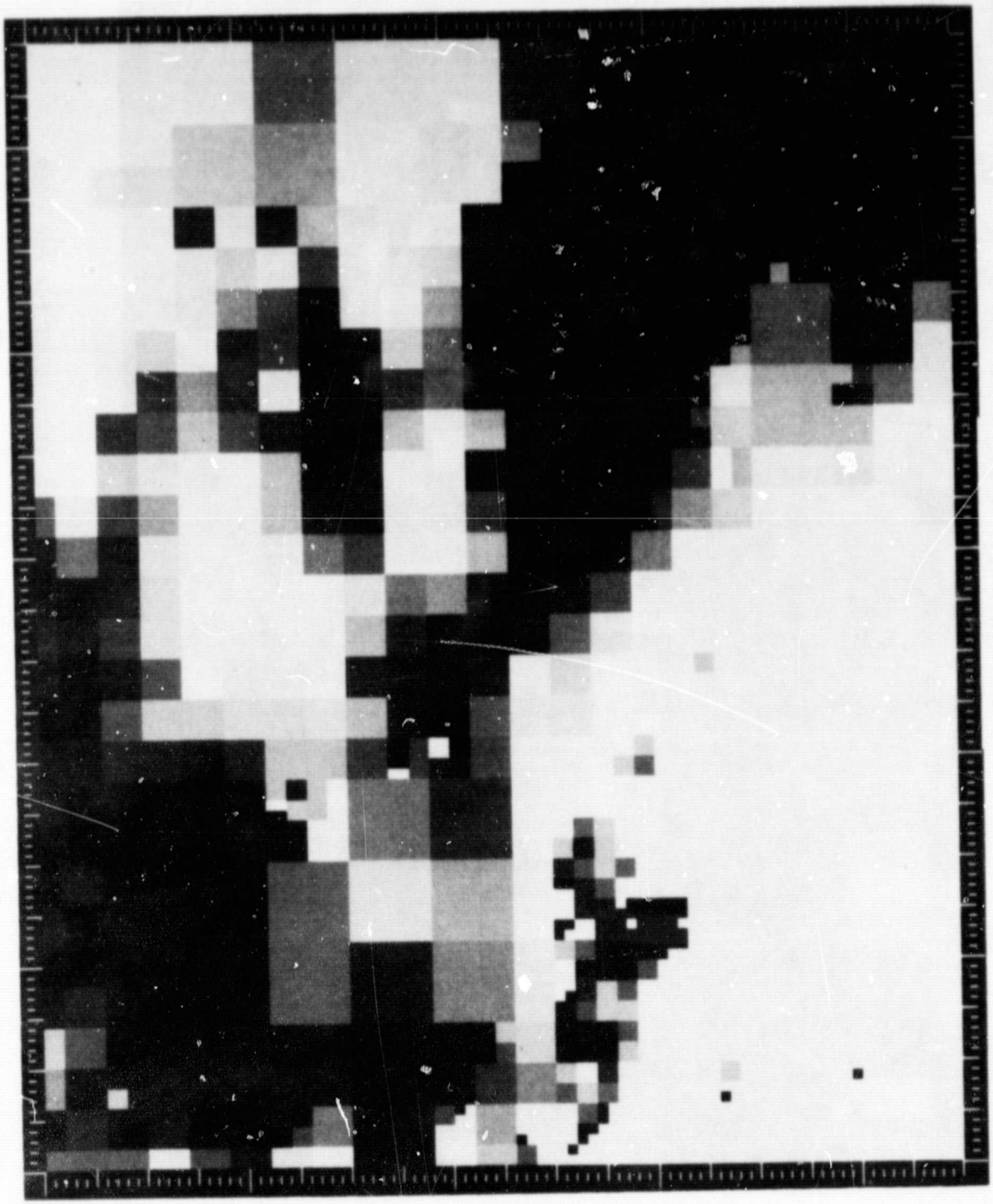

Figure 6-7. The figure displays cloud coverage statistics for one GOES acquisition. A cell with 100% cloud cover is painted white.

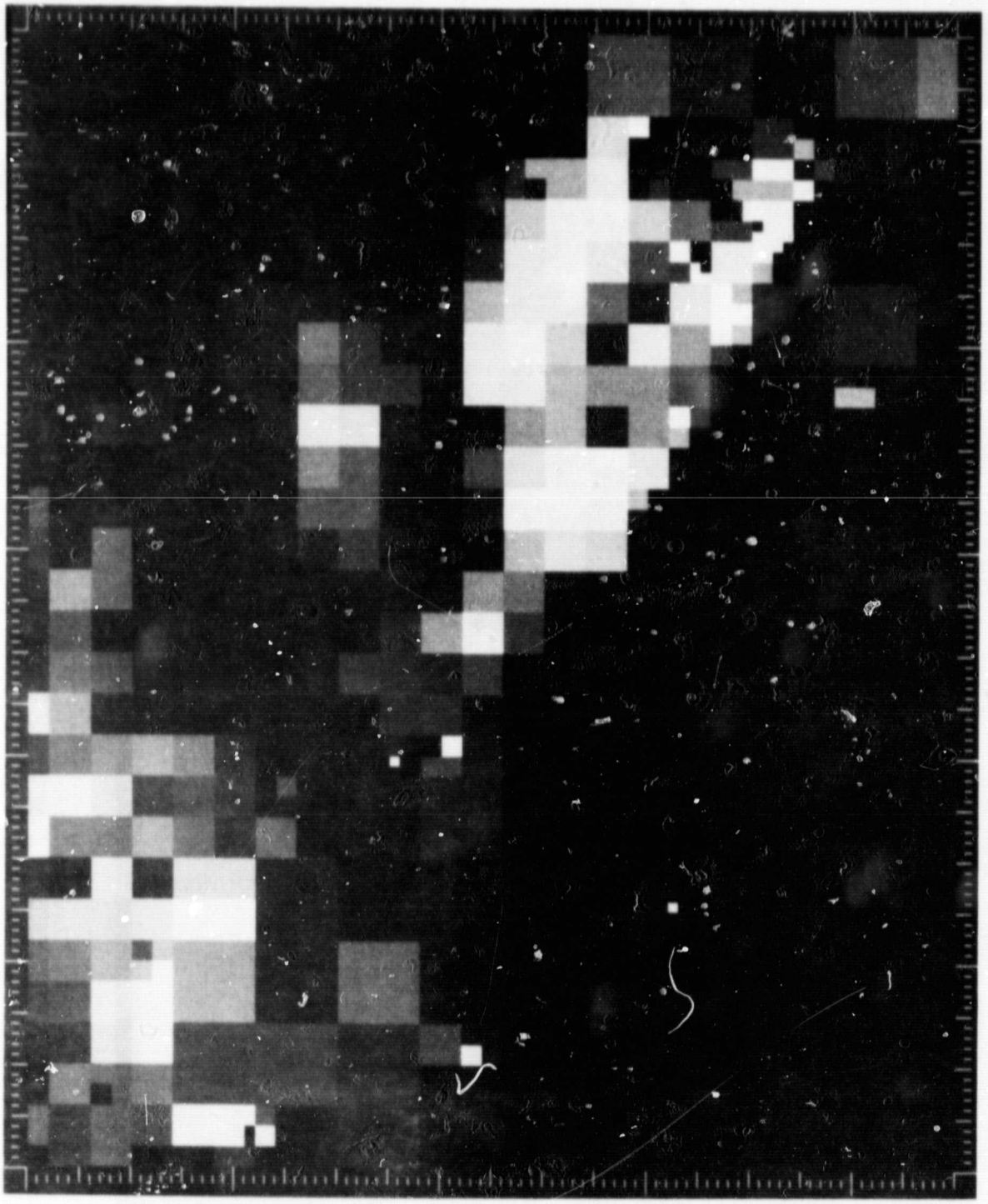

Figure 6-8. The figure displays cloud shadow statistics for one GOES acquisition. A cell with 100% shadow is painted white.

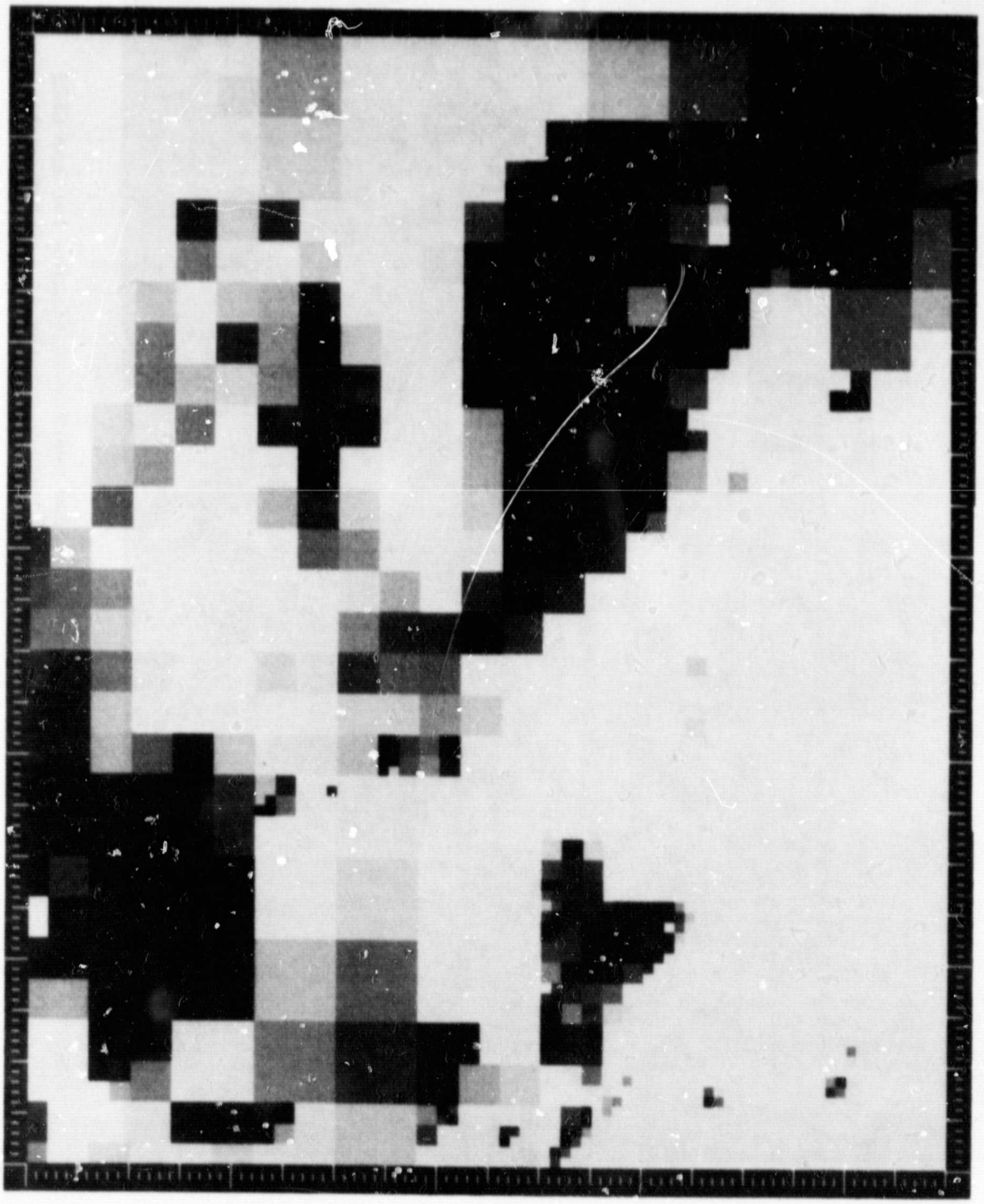

Figure 6-9. The figure displays cloud opacity statistics for one GOES acquisition. A cell that is 100% opaque is painted white.

Figure 6-10. The figure displays cloud shadow opacity statistics for one GOES acquisition. A cell with 100% shadow opacity is painted white.

reasonable and practical. A change in test site or expansion to a larger study area (i.e., entire United States) would certainly require adjustments in some of the numeric assumptions, but the basic model appears practical and expandable for a wide variety of uses.

With the present system configuration, expansion to a continental United States data base is limited by the number of rows in an IBIS column which is currently 10,000. Expanding the current 3.6 km cloud cover model to the continental United States would require approximately 600,000 rows. This can be reduced to 150,000 if a 7.2 km pixel resolution is adopted. It is likely that a 7.2 km basic resolution for cloud cover would prove to be quite acceptable for most insolation uses. Currently, IBIS is undergoing a software expansion, scheduled for completion in late 1983, which will be increasing its processing capacity to 100,000. This would require a 7.2 km continental US data base to be split into East and West components, which is consistent with the current GOES configuration of two satellites (East and West) viewing the United States.

The cloud cover model system has considerable potential for automation. The key obstruction to automation--frame-to-frame registration--is well handled by IBIS procedures. Considerable modelling has yet to be performed before the automation step should be attempted, but no apparent obstacles are foreseen.

The VICAR/IBIS system is designed to enable generation of a multitude of final products. In addition to the tabulation summaries (Appendix II), MAPGEN hardcopy prints, and satellite image prints, generated cloud data can be reported and displayed for specific times, or averaged over any desired period of time. The data can also be contoured and converted to vector (graphics) format if desired.

SECTION 7

ESTIMATING SOLAR RADIATION FROM GOES IMAGERY

A. INTRODUCTION

An important application of cloud parameterization as described above is to estimate incoming solar radiation (insolation) at the surface. Successful modelling of insolation at high spatial and temporal resolution would be beneficial for solar energy and agricultural applications as well as providing information useful for climatological study and forecasting. Numerous works in the area of satellite insolation assessment have utilized the relationship between observed brightness/reflectance and upwelling radiation for modelling albedo and radiation at the ground (e.g., Fritz, et al., 1964; Hanson, et al., 1967; Vonder Haar, et al., 1975; Rockwood and Cox, 1978; Reynolds, et al., 1978; Tarpley, 1979; Raschke and Preuss, 1979; Gautier, et al., 1980; Hiser and Senn, 1980; Norton, et al., 1980; Preuss and Geleyn, 1980; Brakke and Kanemasu, 1981; Diak, et al., 1981; Gautier, 1982; Kowalik, et al., 1982). In addition, a great deal of atmospheric study has been conducted examining the inverse problem--given the satellite and surface measurements, to determine the characteristics and properties of the atmospheric column (for example, Fymat and Zuev, 1978).

In general, the models for incident radiation at the ground are based on either 1) physical consideration of the atmospheric column or 2) the strength of statistical relationships between radiation as a dependent variable and independent variables such as satellite observed brightness, solar zenith angle or other angular positions. This study examines a model from the first category--a physical model. This is not to imply that statistical models cannot contribute significantly to the estimation of solar radiation. However, such "curve-fitting" approaches must be calibrated with

historical ground based measurements. It is not clear from a large-scale database perspective that such calibrations would be stable over time because they depend, in part, on global weather trends, latitude variations, and regular instrument maintenance and calibration. These subjects require further examination. Calibration uncertainties combined with promising results in the physical modelling area (Raschke and Preuss, 1979; Gautier, et al., 1980) led to the selection of a physical model for demonstration purposes.

The remainder of this Section involves the description of the model outlined by Gautier, et al., 1980. The model assumes a plane parallel atmosphere as shown in Figure. 7-1. There are two submodels, one for a clear atmosphere and one for a cloudy atmosphere (stratiform low and middle clouds).

B. THE CLEAR-AIR MODEL

The clear-air model is given by:

$$SW = F_o(1 - \alpha)(1 - a(u_1))(1 + A\ \alpha_1)$$

where

SW	=	clear atmosphere incident shortwave radiation (W/m^2)
F_o	=	instantaneous shortwave solar radiant flux at the top of the atmosphere ($=I_o \cos\ \theta\ W/m^2$)
α	=	reflection coefficient for beam radiation (dimensionless)
α_1	=	reflection coefficient for diffuse radiation (dimensionless)
$a(u_1)$	=	absorption coefficient for slant water vapor path u_1 adjusted for sun angle
A	=	surface albedo (dimensionless, ratio of outgoing to incident flux)
θ	=	zenith angle of the sun

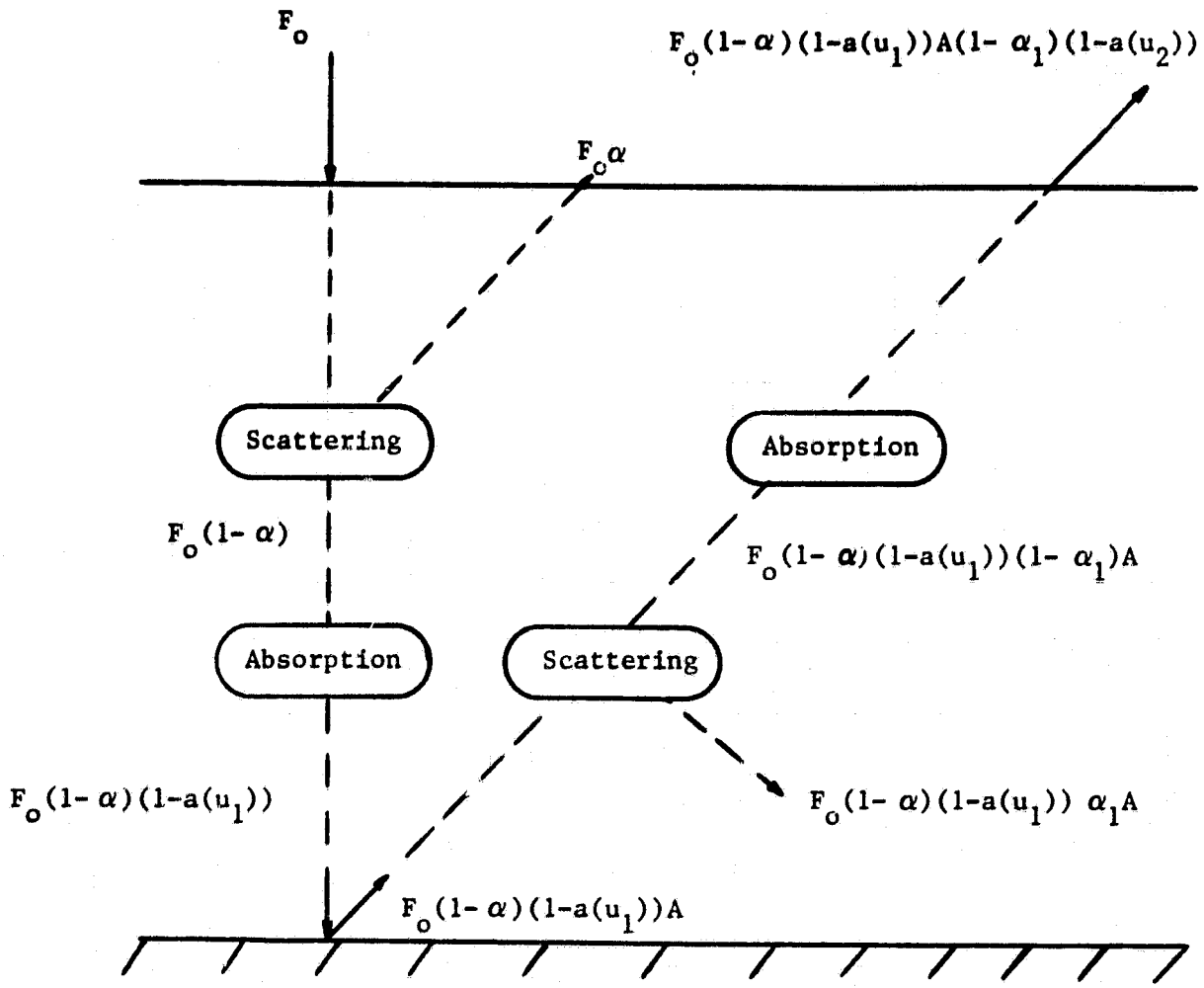

Figure 7-1 Plane-parallel Atmosphere Model

The solar constant is taken here as 1377 W/m^2. The reflection coefficients α as a function of zenith angle and α_1 were taken from Coulson (1959). The scattering from the ground is assumed to be isotropic. The water vapor path length is a parameterized function of latitude derived from Smith (1966). The absorption due to water vapor is taken from Paltridge (1976) which is originally from Lacis and Hansen (1974). The surface albedo for the clear-air case is obtained by translating the actual digital counts (brightness) into reflectance using a calibration equation developed by Norton, et al., (1980). Gautier, et al., (1980) imply that surface albedo is calculated from a function of upwelling radiation and atmospheric parameters, but actually the definitional structure of the model utilizes the planetary albedo measured by the satellite for the pixel(s) of interest (see Gautier, 1982, p. 52) which is then used to calculate surface albedo. The parameterizations used are listed below.

Extraterrestrial radiation on a horizontal surface, F_o: The expression for the F_o is a fundamental calculation given by:

$$F_o = 1377 \; r \cos(\text{zenith angle}) \; W/m^2$$

where

I_o = solar constant (1377 W/m^2)

zenith angle = arcos[cos(latitude)cos(declination)cos(solar hour angle) + sin(latitude)sin(declination)]

r = ratio accounting for variation in sun-earth distance

= 1.00011 + 0.034221cos(t) + 0.00128sin(t) + 0.000719cos(2t) +.000077sin(2t) where t = (Julian day number)x2 π/365

Reflection coefficient for direct radiation, α: Using the curve from Coulson (1959), an exponential least squares fit was derived.

$$\alpha = 0.0502 \exp[2.0570 \; (1 - \cos(\text{zenith angle}))]$$

(correlation coefficient $r^2 = 0.93$ $(r = 0.97)$)

The weakness of this parameterization is the assumption of a Rayleigh atmosphere, an assumption that is often incorrect.

Water vapor absorption, $a(u_1)$: There are three steps to this calculation. First, the precipitable water vapor path length must be computed. There are a number of approaches that have been suggested (Reitan, 1963; Benwell, 1965; Bolsegna, 1965; Smith, 1966; Lowry and Glahn, 1969; Idso, 1970; Karalis, 1974). The one adopted by Gautier, et al., is the Smith (1966) parameterization. This model is a function of dew-point temperature, season, and latitude:

$$\text{water vapor path length} = \exp[0.1133 - \ln(\lambda + 1) + 0.0393\, T_d]$$

where λ = mean moisture profile parameter (=3.11 here)

T_d = mean dew-point temperature (=44.9 here)

Recent work by Viswanadham (1981) examined a number of such models (including Smith's) and concluded that "...estimates of precipitable water from mean monthly surface dew-point temperatures are not sufficiently reliable to justify making surface measurements to infer existing precipitable water. And, for those stations and conditions, where a significant correlation does not exist between surface dew-point and total precipitable water, the predicting equation has no value. (p. 8)" Until this conflict is resolved, it is unclear whether the use of such a parameterization is appropriate.

Given the preciptable water vapor, the second step is to adjust it for current sun angle position in order to account for the variation in path length during the day. This is done by dividing by the cosine of the zenith angle. Third, the actual water vapor absorption is calculated using Lacis and Hansen's (1974) result:

$$a(u_1) = 2.9u_1/[1 + 141.5)^{0.635} + 5.925u_1]$$

The relationship given above approximates absorption at standard temperature and pressure (STP) to better than 1% accuracy over the range of water paths 10^{-2} to 10 cm. Paltridge (1973, 1976) has suggested a linear pressure correction and a square root temperature dependence for non-STP situations. However, the use of such corrections is believed to have minimal impact for most atmospheres (e.g., the temperature adjustment is not highly significant since the range of absolute temperature is not great within the atmosphere and the pressure corrections suggested have been limited to simple linear corrections). No corrections were applied to the water vapor absorption parameterization used here.

Diffuse reflection coefficient, α_1: The value for this parameter was obtained from Paltridge (1976, p. 126):

$$\alpha_1 = 0.28/(1 + 6.43 \cos(\text{zenith angle}))$$

This formula is accurate to 1% assuming a Rayleigh standard atmosphere above a blackbody earth. The equivalent planetary albedo integrated over all sun angles for a clear atmosphere with standard ozone and for the complete solar spectrum is 6.22%. Coulson's 1959 value of 6.9% underestimated ozone absorption (Paltridge, 1976).

Surface albedo, A: The surface albedo is obtained from the satellite brightness measurements and calibrated to a reflectance scale using the following expression (Norton, et al., 1980):

$$\text{Reflectance} = (\text{Digital Counts}/63)^2$$

Visible data are stored on magnetic tape in the resolution specified by the operator at the time of recording as 6, 7, or 8-bit data dependent upon the resolution. Prior to transmission, all data are converted to 8-bit data to obtain maximum contrast. Thus 6-bit data are shifted by 2 bits to create 8-bit (0-255) data (Staton, 1982). For the present study, the 63 in the

denominator was replaced with 255 to calibrate the digital numbers. In order to obtain the directional reflectance the satellite observed reflectance was divided by the cosine of the angle between the sun and the satellite. Using spherical trigonometry, the cosine value is:

$$\cos(a) = \cos(\theta)\cos(s) + \sin(\theta)\sin(s)\cos(\beta - \gamma)$$

where

$\cos(a)$ = cosine of angle between sun and satellite

θ = solar zenith angle

s = satellite zenith angle (90^{o} - latitude)

β = solar azimuth angle

γ = satellite azimuth from north = satellite longitude - ground longitude + 180^{o}

The digital counts were obtained for four cells within the test area and are labeled here in correspondence with the ground measurement stations: Alhambra, Barstow, Ridgecrest, and San Diego. A computer program was written to implement the above model, and using April 3, 1980 as an example of a clear atmosphere, the model was run for each site. Runs were made using the actual pixel in which the ground instrument was located and also the averaged digital counts for the overall cell if the grid size was larger than the minimum 4 x 4 km. The grid cells and the relative positions of the instruments are shown in Figure 7-2. Although San Diego was labeled on Figure 7-3 and data from it were to be used in the analysis, the presence of high altitude cirrus clouds confounded the model results. This will be discussed further in the Section on the cloudy atmosphere model which follows.

Results of these runs are illustrated in Figures 7-4 - 7-6. All times were registered on Greenwich Mean Time (GMT) and converted to solar time suitably adjusted for longitude and the equation of time. The time scales of

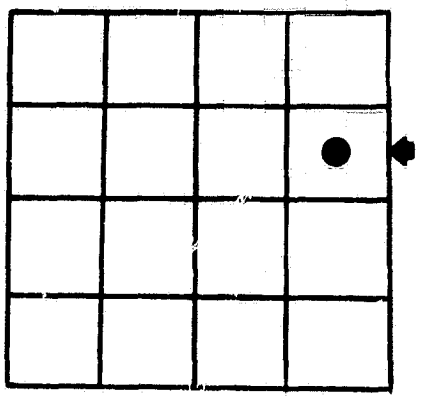

Figure 7-2a. Ridgecrest, CA; latitude = 35° 37'; Longitude = 117° 40'.

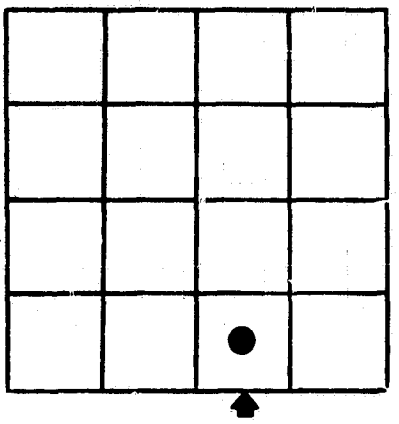

Figure 7-2b. Barstow, CA; Latitude = 34° 53'; Longitude = 117°.

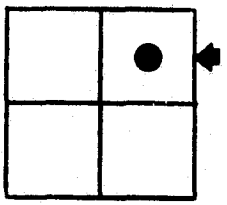

Figure 7-2c. Alhambra, CA; Latitude = 34° 5'; Longitude = 118° 9'.

Figure 7-2. These figures indicate the pixels in which pyranometers are located at selected stations with respect to the georeference grid cell definitions.

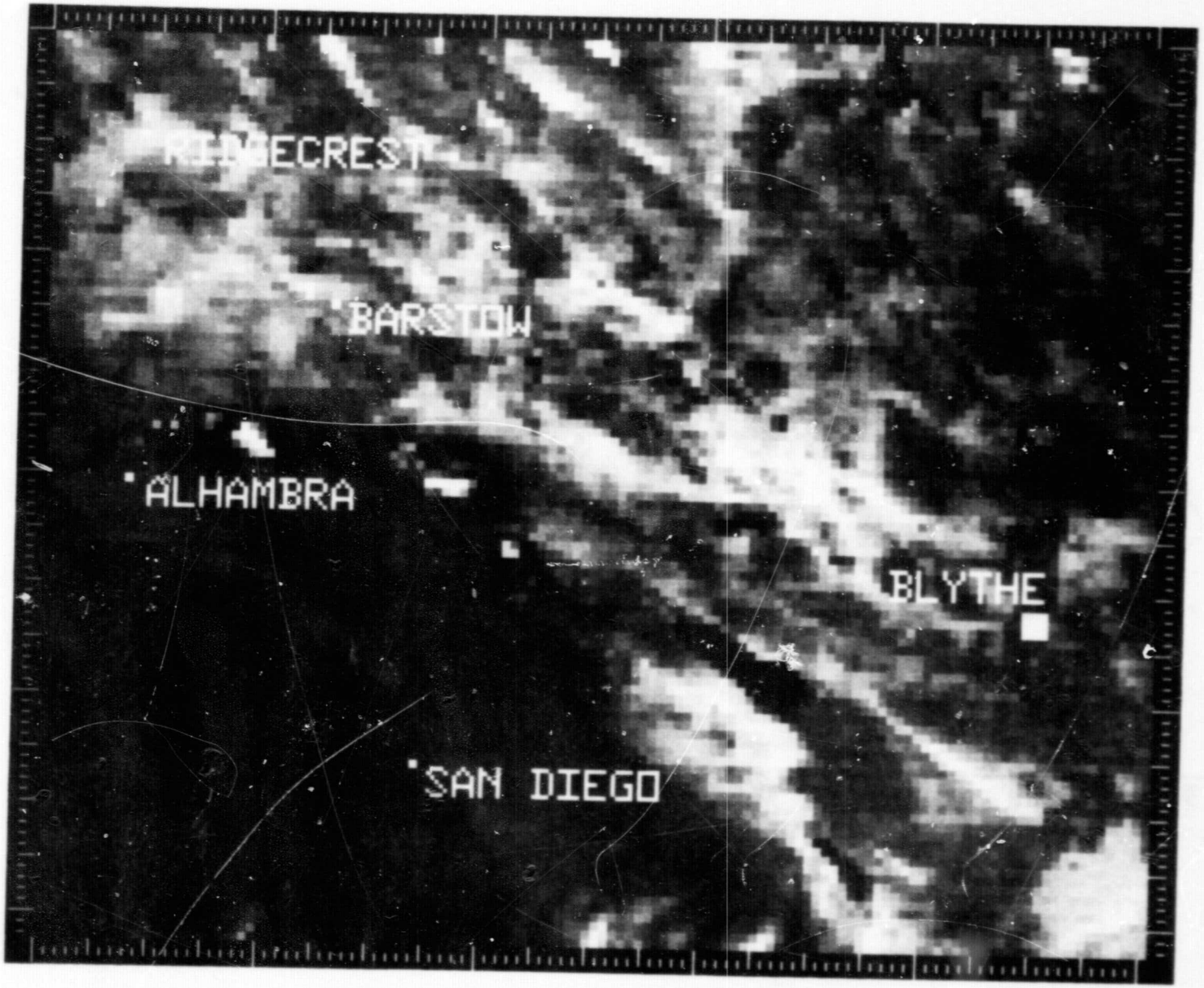

Figure 7-3. The figure indicates station locations from which insolation data were used in the model evaluation. Although hard to discern, the GOES pixel in which the pyranometer is located has been enhanced (bright white).

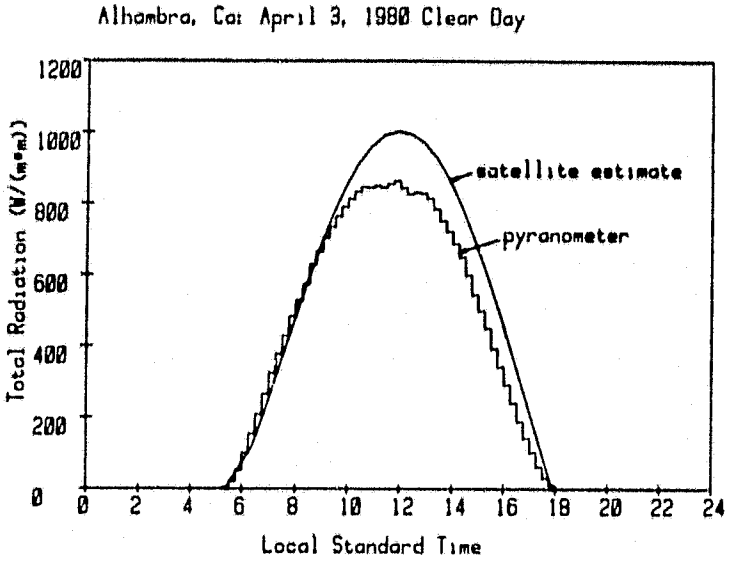

Figure 7-4. Plot of satellite estimate and actual pyranometer readings on a clear day at Alhambra, CA. Grid cell resolution is 13 km^2.

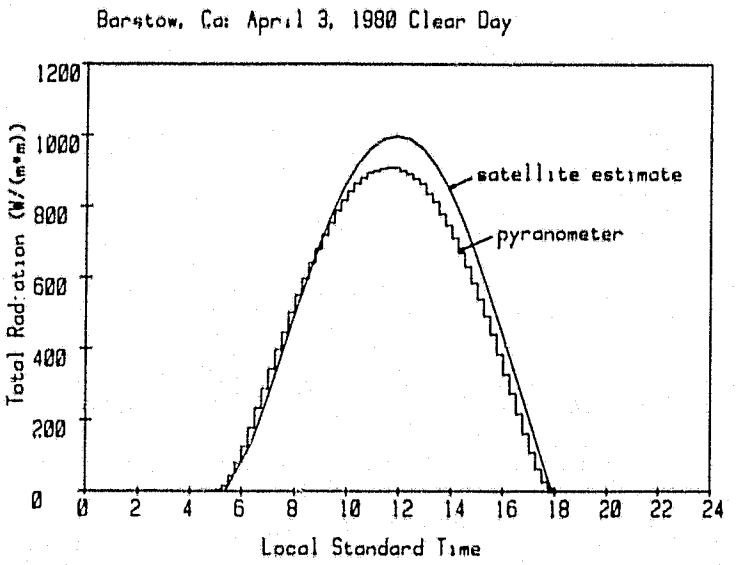

Figure 7-5. Plot of satellite estimate and actual pyranometer readings on a clear day at Barstow, CA. Grid cell resolution is 13 km^2.

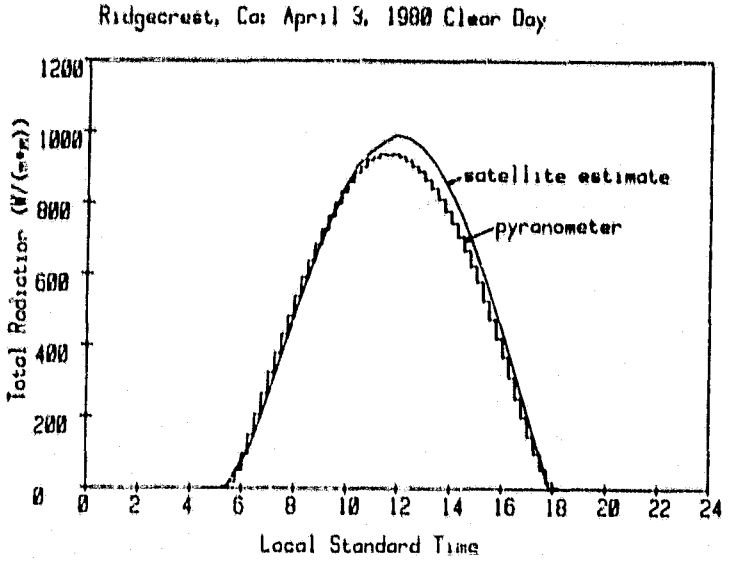

Figure 7-6. Plot of satellite estimate and actual pyranometer readings on clear day at Ridgecrest, CA. Grid cell resolution is 13 km^2.

the figures are all in local (Pacific) standard time (GMT - 8). The pyranometer measurements represent averages over the previously recorded 15-minute interval (15, 30, and 45-minutes after the hour and on the hour). The satellite begins recording the image at 15 and 45-minutes past the hour taking 18 minutes for the full earth scan. For the purposes of this study it was assumed that the digital counts for the areas of interest were recorded, on average, at the midpoint for the 15-minute interval of transmission. The calculation of the exact time of recording is complicated by a 4.5^{o} movement in sun angle during this period. The geometry involved in the satellite estimates were based on the midpoints of the 15-minute interval. Detailed calculations for actual recording times were not performed within the study although this could be done.

It should be noted that the GOES satellite images in the spectral range 0.52 to 0.72 μm while the pyranometer measurements are integrated over the entire spectrum. In a manner similar to Gautier, et al., 1980, the satellite data were spatially averaged over a 4 x 4 km. pixel box (instead of 8 km x 8 km. as in Gautier, et al., 1980) to partially account for time and angle discrepancies. Radiative transfer models could possibly be used to transform the spectral radiances to broad band solar fluxes (not attempted within this study).

The curves shown in Figures 7-4 - 7-6 illustrate total horizontal insolation for the ground based instrument and the satellite modelled value for Alhambra, Barstow, and Ridgecrest. The satellite values presented here have a resolution of 4 km x 4 km. The values between sunrise and 0630, and between 1600 and sunset are extrapolated. The results are in remarkable agreement with surface measurements.

However, closer inspection of the functional form of the clear-air model reveals that the primary determinant of the agreement is the cosine behavior of the F_o term. That is, the combined effect of the direct reflection and water vapor absorption terms typically reduces extraterrestrial radiation on the order of 10-30% with the shape of the curve being driven by the cosine function. Even more interesting is the lack of sensitivity to the satellite measurement as evidenced in the clear-air model. Note that the direct component is multiplied by a $(1 + A\ \alpha_1)$ term (direct + diffuse components). Even if both the diffuse reflection and surface albedo were 0.30, the maximum impact on the clear-air estimate would be only 9%. Since the typical value found by Coulson for the diffuse reflection was 6-7%, the impact of the satellite input on the clear-air model is minimal and large errors can be tolerated with little effect on curve-fitting to ground-truth data.

Claims of errors under 10% (Gautier, et al., 1980; Tarpley, 1979; Brakke and Kanemasu, 1981) must be considered in view of the fact that the clear-air model is relatively insensitive to variations in the satellite observed surface albedo and the fact that insolation is not normally distributed, thus confounding the use of standard deviations for error analysis (Hanson and DeLuisi, 1981). The derivation of an appropriate measure for such comparisons is beyond the scope of this study so only the graphical results are presented here. In addition, the location of surface measurements and their representativeness of the grid cells was not addressed.

Note that the curves for Alhambra incur greater error during the mid-day period. We believe this is due to significant air pollution or marine air effects in the Los Angeles Basin which increase absorption and scattering (Gammon, et al., 1981). This reflects a weakness of the water vapor absorption parameterization taken from Paltridge (1976). In his 1973 paper, Paltridge obtained measurements under dense haze which are significantly different (see his Figure 4, p. 159) from clear-air conditions implying the water vapor absorption model needs modification to account for haze conditions. An alternative would be to signal, through the satellite measurements, when the clear-air model assumptions might be invalid due to haze. Again such activity is recognized but is beyond the scope of this study. The effects of smog and naturally occurring atmospheric haze also appear in the traces of actual measured data. The clearest atmosphere is above Ridgecrest, followed by Barstow and then Alhambra. At Barstow, pollutants and/or marine air advected into the high desert from the Los Angeles Basin result in approximately a 40 W/m^2 lower value at Barstow than at Ridgecrest, but Barstow still has a 35 W/m^2 higher value than Alhambra, located in the Los Angeles Basin.

The measured value at Ridgecrest is 95% of the estimated value, while it is only 88% for Alhambra. The latter station has a smaller percentage because of the effects of aerosols in the local atmosphere that were undetected, using our methodology, on the satellite image and therefore a clear day estimate was calculated.

Because of the insensitivity of the clear-air model to the digital counts, the results obtained using averaged digital counts for the entire grid cell are not included here (they were virtually identical within 10-20 W/m^2 in the worst case).

C. THE CLOUDY ATMOSPHERE MODEL

The cloudy atmosphere model is more complex because assumptions must be made regarding the percentages of water vapor above and below the clouds. The cloud model assumes an average of 30% of water vapor above cloud level and 70% below. These estimates are based on work by Paltridge (1973). The model, because of its Rayleigh atmosphere construction assumes homogeneity and spherical molecules within the atmospheric column. The complexity of this problem has been reviewed to some extent in Liou, 1976; Reynolds, et al., 1975, 1978; Twomey, 1970, 1976, 1978; Davies, 1978; and Stephens, et al., 1978. The incident short-wave radiation relationship for the cloudy-air model is given by:

$$SWC = F_o(1 - \alpha)(1 - a(u_1)_t)(1 - A_c)(1 - abs_c)(1 - a(u_1)_b)$$

where

SWC = incident shortwave radiation (W/m^2) at the surface under a cloudy atmosphere

$a(u_1)_t$ = water vapor absorption of incident radiation above cloud

$a(u_1)_b$ = water vapor absorption below cloud

abs = cloud absorption (dimensionless)

A_c = cloud albedo

All other variables are as defined in the clear-air model. Gautier, et al., 1980, use the brightness measurement together with the minimum surface albedo to determine the presence of clouds--that is, a cloud threshold. The minimum surface albedo is obtained by examining several clear day images and forming a composite day profile of minimum surface albedo images. The approach used in this study for determining the presence of clouds has been described. The differences between using the threshold approach and our approach are unclear due to insufficient details given in Gautier, et al., (1980, 1982) regarding the "confidence margin" utilized in establishing the threshold. The approach developed in this study was used to determine whether the atmosphere was clear or cloudy and the percent of coverage. The parameterizations used in the model are described below.

Water vapor absorption above the cloud top (t) and below the cloud (b); $a(u_1)_t$, $a(u_1)_b$: The only difference between these elements and the one in the clear-air model is that, on average, 30% of the water vapor is assumed to be above the cloud. Thus, we simply multiply the precipitable water vapor by 0.30 and then substitute this new value in the water vapor absorption function $a(u_1)$ described for the clear-air case. In a similar fashion, the remaining 70% assumed to be below the cloud is applied to the precipitable water vapor and that value is substituted in the same water vapor absorption function. The procedure is repeated for the surface-to-satellite water vapor path.

Cloud absorption, abs: Cloud absorption was assumed to be a linear function of brightness ranging from zero for no cloud to a maximum of 0.2 for

thick clouds (Reynolds, et al., 1975; Stephens, et al., 1978; Gautier, et al., 1980). This simplified approach was chosen because of uncertainties in the mechanisms responsible for larger absorptions (type, size, and shape of particles; Liou, 1976; Twomey, 1970, 1976). The parameterization used was:

$$\text{abs} = \begin{cases} 0.0 & \text{if BR} < 0.5 \\ \text{BR} - 0.49 & \text{if } 0.49 \leq \text{BR} \leq 0.67 \\ 0.2 & \text{if BR} > 0.67 \end{cases}$$

Cloud albedo, A_c: The derivation of the cloud albedo is more complex. It can be shown that the upwelling radiation detected by the satellite over a cloudy atmosphere is a quadratic function of atmospheric parameters, surface albedo, and upwelling radiation at the satellite. The resulting quadratic may be solved for cloud albedo under certain conditions. However, during the present study, a number of situations occurred where the upwelling radiation was close in value to the component reflected by the atmosphere ($F_o \ \alpha_1$). In those cases, the resulting solution consisted of two negative roots. This problem is believed to be caused by the lack of a uniform cloud layer as identified in the cloud statistics (percent cloud did not equal 100%). The model outlined by Gautier, et al., 1980, assume stratiform clouds and not finite clouds. Thus, it may be possible to extend this model with the use of cloud statistics to account for finite clouds.

Results of a series of runs made using the cloud model are illustrated by Figures 7-7 - 7-9 at a satellite resolution of 4 x 4 km^2. Note that these plots are extrapolated from sunrise to 0630 and from 1600 to sunset. As in the clear air case, the satellite estimates are assumed to represent the midpoint of the pyranometer time scale and are converted to local (Pacific) standard time. As displayed, the satellite estimates capture the general pattern of insolation. Again, it should be noted that the

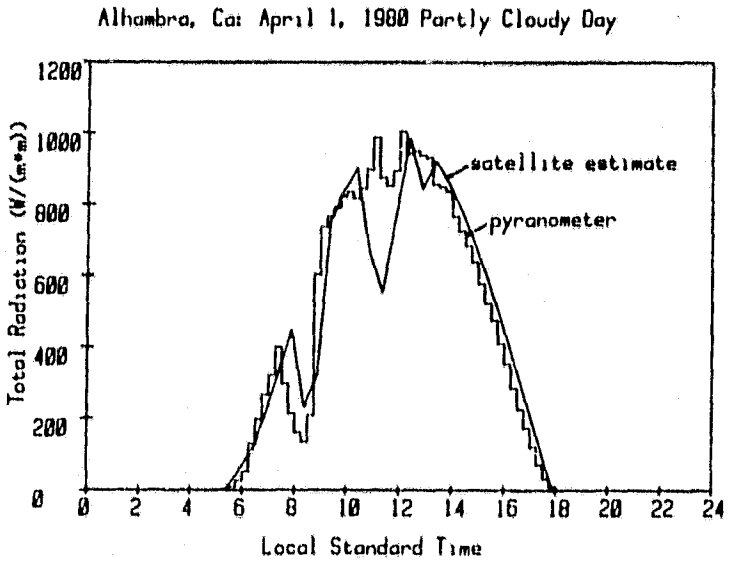

Figure 7-7. Plot of satellite estimate and actual pyranometer readings on a partly cloudy day at Alhambra, CA. Grid cell resolution is 13km^2.

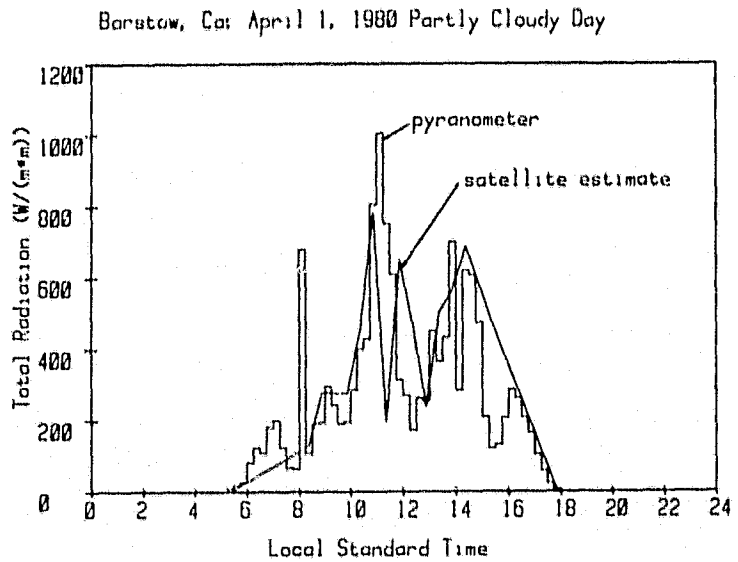

Figure 7-8. Plot of satellite estimate and actual pyranometer readings on a partly cloudy day at Barstow, CA. Grid cell resolution is 13km^2.

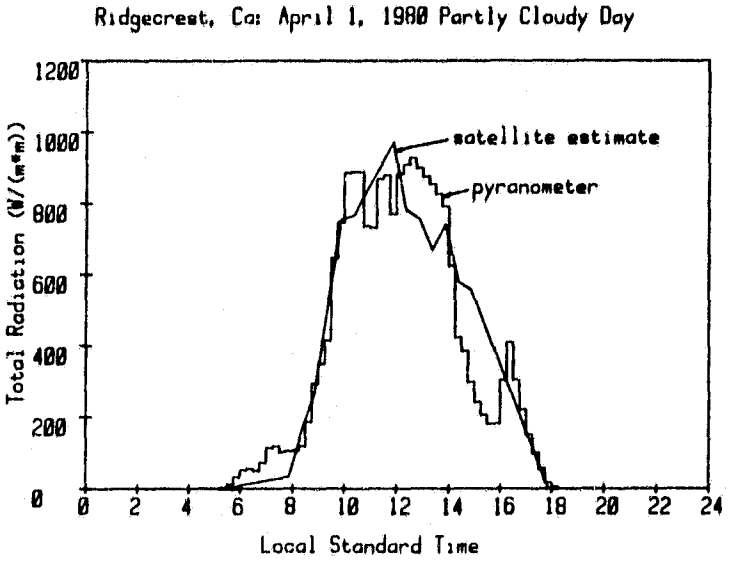

Figure 7-9. Plot of satellite estimate and actual pyranometer readings on a partly cloudy day at Ridgecrest, CA. Grid cell resolution is 13km^2.

satellite values represent two instantaneous recordings per hour whereas the pyranometer values are integrated 15-minute averages. This is particularly evident for Barstow, Figure 7-8, where a large peak insolation value between 0800 and 0815 was "missed" by the satellite which began recording at 0815. The large drops after 1500 were also missed because the model did not generate a solution for the 1545 recording (38% cloud/67% cloud opaque) due to the presence of finite clouds within the grid cell detected by the cloud statistics. Thus the interpolated value drops linearly to sunset. This also occurred with the Ridgecrest data Figure 7-9 (19% cloud/61% cloud opaque). However, the pattern for the other peaks and dips are similar for both the pyranometer measurements and satellite model.

As an additional observation, a case was also run using a site in San Diego, California. Here the presence of high cirrus clouds (Figure 7-10) that are virtually invisible to the naked eye on the photographic image complicated the analysis. These clouds become more visible in the afternoon portion of the April 3 and 4, 1980 image and were detected during the entire day by the cloud statistics algorithm (100% cloud in all samples during that day). High levels of insolation measured at the ground indicate the cloud model needs modification to accurately assess these conditions.

In addition to the above results, a number of related studies were made examining the size of the pixel area and the effects of averaging values. Figures 7-11 through 7-13 illustrate the effect of averaging the digital counts over the original grid cell definitions for each case. These averaged digital counts were then input to the model. The effect of calculating averaged estimates for each pixel and then averaging was not examined in this study. Using parallel cloud statistices for each image sample, a weighted sum for the large-area grid cells was computed. The cloud model estimates for the large grid cells were calculated using:

$$SWC_{gc} = (1 - PCLDY)\ SW + (PCLDY)\ SWC$$

where

SWC_{gc} = short-wave radiation as weighted sum of clear and cloudy estimates under partly cloudy atmosphere

PCLDY = percent cloud from cloud statistics data (1-PCLDY = percent clear by definition)

SW = incident short-wave radiation under clear atmosphere

SWC = incident short-wave radiation under cloudy atmosphere

As expected, the detail obtained at the averaged pixel resolution is not as good since in the Barstow and Ridgecrest cases the estimates represent

Figure 7-10. GOES image of 4 April 1980 (1845 GMT) showing high cirrus clouds and atmospheric haze.

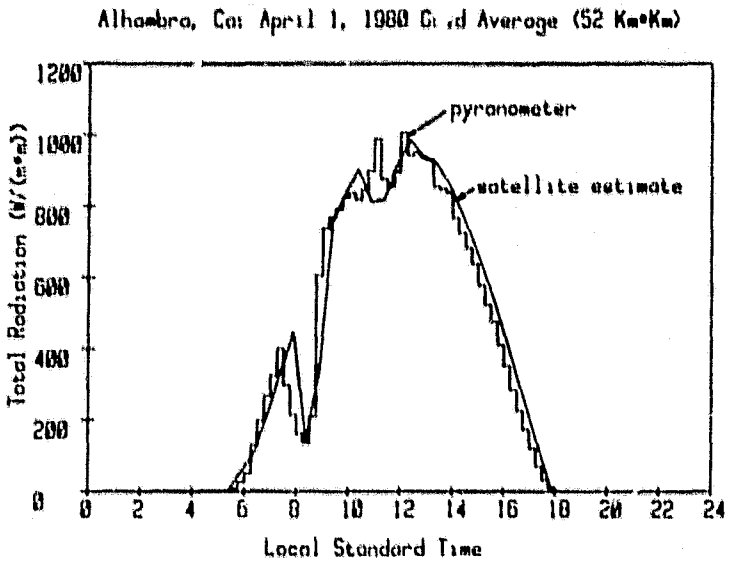

Figure 7-11. Plot of satellite estimate and actual pyranometer readings on a partly cloudy day at Alhambra, CA. Grid cell resolution is 52km^2.

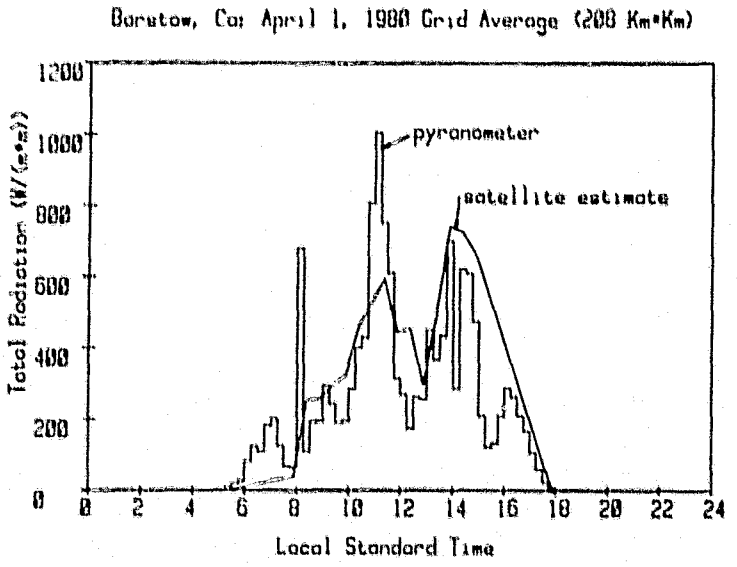

Figure 7-12. Plot of satellite estimate and actual pyranometer readings on a partly cloudy day at Barstow, CA. Grid cell resolution is 208km^2.

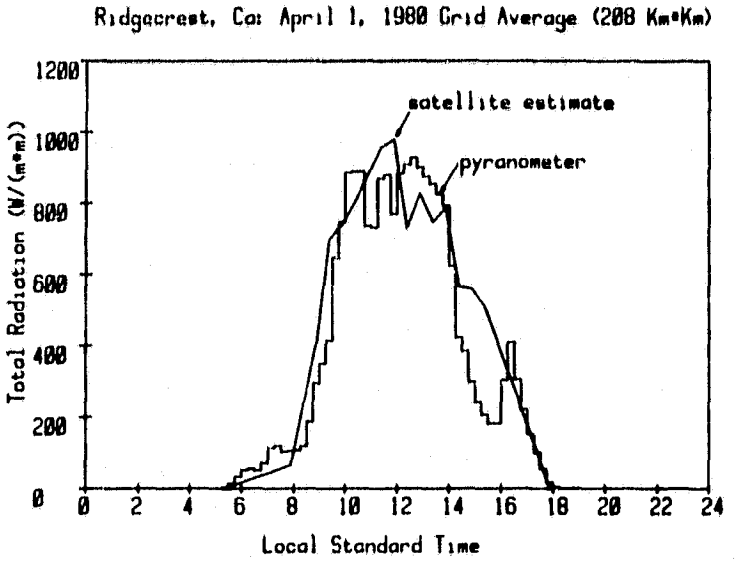

Figure 7-13. Plot of satellite estimate and actual pyranometer readings on a partly cloudy day at Ridgecrest, CA. Grid cell resolution is 208km^2.

a 208 km^2 area while the pyranometer measurements are point estimates. The Alhambra estimates are actually improved by enlarging the area to 52 km^2. It is not clear whether this improvement is due to cancellation of errors due to averaging or a more homogeneous representation of the atmosphere since the Alhambra area has less local relief than the larger cells. The differences in the clear-air case between the small and large grid cell areas were minimal. This may have been due to the homogeneity of the larger cells since they were selected to be climatologically similar regions.

Finally, two cases under cloudy conditions were prepared using hourly time intervals--one at 13 km^2 and one at 208 km^2 resolution. The four pyranometer estimates during each hour were averaged and the two satellite

estimates were averaged. Examining Figures 7-14 and 7-15, the profile at the finer resolution follows the surface measurements more closely than the averages for the larger grid cell. These results indicate that more accurate estimates may be obtained at the 4 x 4 km resolution rather than the 8 x 8 km resolution suggested by Gautier, et al., (1980). Using the variable grid cell area capability available with the VICAR/IBIS software, the flexibility exists to examine some areas at the 4 x 4 km resolution. It is postulated that the larger cell sizes used by Gautier may have been due to the higher latitude at which their cases were run (45^{o} plus).

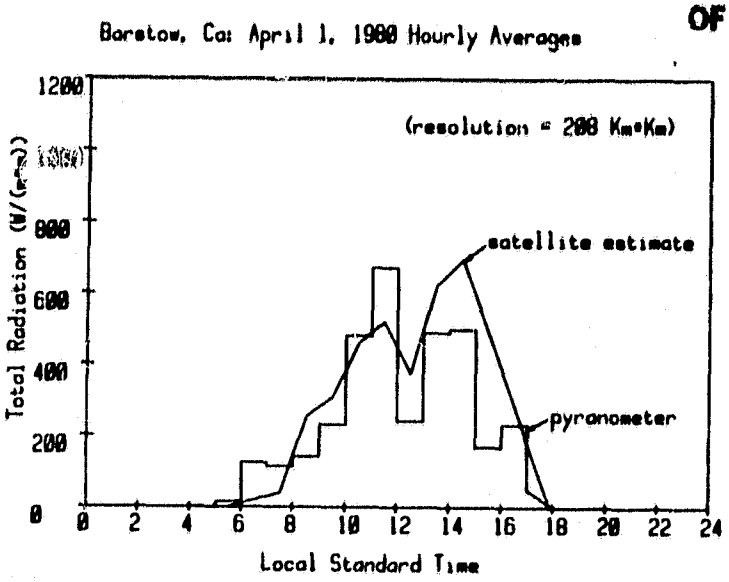

Figure 7-14. Plot of satellite estimate and actual pyranometer readings at Barstow, CA using hourly averages and a grid cell resolution of 208 km^2.

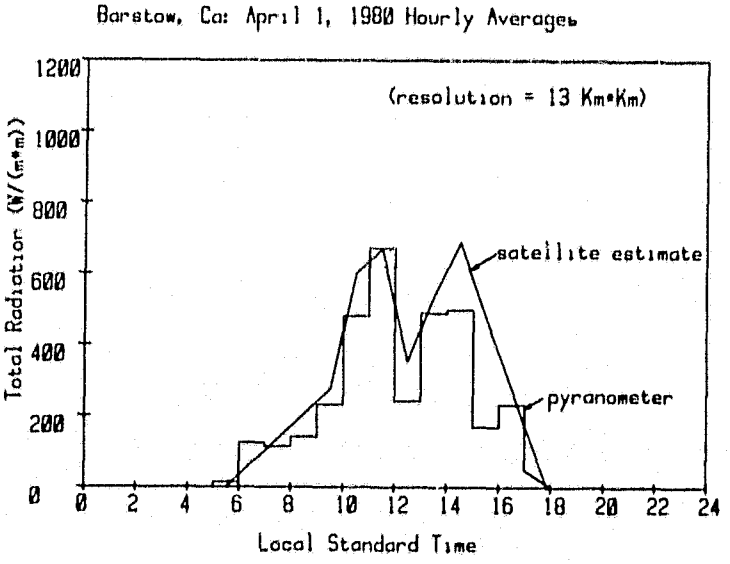

Figure 7-15. Plot of satellite estimate and actual pyranometer readings at Barstow, CA using hourly averages and a grid cell resolution of 13 km^2.

SECTION 8

DISCUSSION AND CONCLUSIONS

Results of the completed research suggest that development of an operational system to establish long-term cloud cover attribute statistics at a high spatial resolution and for large geographical areas is feasible with current technology. The system could provide detailed cloud cover attribute statistics to help refine insolation estimation models, and to increase our understanding of temporal and spatial variations of cloud cover. As often stated, with clear sky conditions, the amount of insolation available to solar systems varies little between sites. It is with different types of cloud cover that significant insolation variations occur.

Techniques used in this research to identify and map cloud attribute statistics are not considered optimal, and in any operational system they would require refinement and some additional development. The basic methodology, however, appears applicable.

The concept of climatic regionalization and the use of a variable grid cell size are two factors that can significantly reduce the cost of computer time required to generate cloud cover statistics for large areas and on a regular basis. System automation is also feasible and would further reduce operational costs.

With respect to insolation estimation procedures that have been used, there are a number of shortcomings that need to be addressed. First, the insensitivity of the clear-air model to the satellite input implies that the other coefficients in the clear-air model need to be precise because their effect is to shift the cosine curve up and down proportionately. Because one of the coefficients is derived from a Rayleigh atmosphere, a limitation of the

model is possible, especially in those areas where a non-Rayleigh atmosphere is typical. Much research has been conducted since the cited work of Coulson (1959) and include Paltridge, 1976, and Fymat and Zuev, 1978. Improvements to the model's sensitivity might be achieved by utilizing results of these studies. It has been argued that Rayleigh scattering is sufficient for an "average" atmosphere, but in those locations and situations where user requirements dictate hourly estimates for correlation with other types of ground-based measurements (such as utility load data), a mean value may not be acceptable. Thus far, the majority of satellite-insolation studies have been on a case-by-case basis. No long term data are available as to the reliability or accuracy of insolation estimates using this approach.

Second, no consensus exists on the water vapor path length calculation and its appropriateness (Viswanadham, 1981). It may be that the sensitivity of the short-wave radiation to it is low. Nevertheless, the parameterization used should be consistent with theory and current data.

Third, the capabilities of the model under polluted, hazy, or partly cloudy atmospheres need additional examination. Cloud statistics can be generated to aid in cloud definition and presence, as was demonstrated in this study. Other approaches to such statistics have also been demonstrated (McCleese, 1981; Logan, et al., 1982).

Fourth, additional research is recommended to understand the proper characterization of error between ground-truth data and satellite estimates. More exact time calculations could be made and at a finer pyranometer network resolution (e.g., a large number of insolation measuring stations are located in the Los Angeles Basin).

Fifth, differences in using larger pixel areas or hourly averages are trade-offs between user needs and time-scale requirements. If only total

daily estimates are required, the hourly images are still necessary in order to perform the summation to daily totals. If hourly discrimination is needed, the half-hourly values could be calculated and summed, or one sample per hour could be assumed to represent the entire hour. The risks of the latter approach are clearly demonstrated in Figures 7-8 versus 7-15 for Barstow, characteristically a clear site. This is a trade-off between user needs and system costs that needs to be addressed.

In conclusion, a number of points have been demonstrated in this study:

(1) A variable grid cell can be effectively used to reduce the amount of computer time required to read, analyze and display cloud cover attribute statistics.

(2) The methodology developed lends itself to automation which would further reduce system costs and efficiency.

(3) A physical modelling approach is a viable method for estimating incident short-wave radiation given that it is epistemologically consistent. The physical model used in this study provides reasonable estimates for a limited number of cases. However, there are some structural aspects of the model open to debate, such as the Rayleigh scattering model, the water vapor path length parameterization, the models performance in the presence of non-uniform, finite clouds, and the sensitivity (or insensitivity) to the satellite inputs in the clear-air case.

(4) The amount of additional detail that could be added to such a model is substantial using the VICAR/IBIS software. The implications on computation time for additional model capability were not addressed in detail. The point to be made is that the availability for model expansion exists with the current configuration.

(5) The use of cloud statistics has been shown to be a useful way of estimating the incident short-wave radiation for grid cells containing finite clouds (partially cloudy, non-uniform clouds) as a weighted average of clear-air and cloudy-air estimates.

(6) The model needs to account for certain non-Rayleigh atmospheres containing air pollutants. In the solar energy area, many applications and markets are within or near urban areas. These areas tend to possess levels of pollution which impact system designs in that the insolation resource is an elementary design element. Also of interest are situations where high cirrus clouds are present.

(7) Cloud statistics such as percent cloud and percent cloud opacity provide a more quantitative measure of cloud cover than subjective surface observations. The percent shadow could be used to more accurately calibrate the brightness of the image in the presence of clouds. These cloud statistics could also be used to characterize the presence of smog or high cirrus and possibly signal the use of a third submodel for such conditions.

SECTION 9

REFERENCES

Angelici, G. L., Bryant, N.A., Fretz, R.K., Friedman, S.Z. (1980), "Urban Solar Photovoltaics Potential: An Inventory and Modelling Study Applied to the San Fernando Valley Region of Los Angeles," JPL Publication 80-45, July.

Benwell, G.R.R. (1965), "Estimation and Variability of Precipitable Water," U.S. Dept. of Commerce Weather Bureau Technical Paper No. 10, 48.

Bolsegna, S.J. (1965), "The Relationship Between Total Atmospheric Water Vapor and Surface Dew-point on a Mean Daily and Hourly Basis," J. Appl. Meteor., 4, 430-432.

Brakke, T.W., and E.T. Kanemasu (1981), "Insolation Estimation from Satellite Measurements of Reflected Radiation," Remote Sensing of Environment, 11, 157-167.

Bryant, N.A. and A.L. Zobrist (1976), "IBIS: A Geographic Information System Based on Digital Image Processing and Raster Datatype:, in: Symposium on Machine Processing of Remotely Sensed Data, LARS, Purdue University, West Lafayette, Indiana, June 29.

Bryant, N.A., and A.L. Zobrist (1982), Some Technical Considerations on the Evolution of the IBIS System," in Proceedings, Pechdra VII Symposium, Remote Sensing: An Input to Geographic Information System if the 1980's, Sioux Falls, S.D., 18-21 October 1981, 465-475.

Bryant, N.A., S.Z. Friedman, and J.R. Huning (1981), "A Feasibility Study for the Use of GOES Satellite Data for a Solar Energy Data Base," Satellites and Forecasting of Solar Radiation, Summary of the Workshop Sessions and Additional Papers, A Workshop of the Solar Radiation Division of American Section of ISES, February 2-5, 119-127.

Coulson, K.L. (1959), "Characteristics of the Radiation Emerging from the Top of a Rayleigh Atmosphere, 1 and 2, Planetary Space Science, 1, 256-284.

Davies, R. (1978), "The Effect of Finite Cloud Geometry on the Three Dimensional Transfer of Solar Irradiance in Clouds," J. Atmos. Sci., 35, 1712-1725.

Davis, J.M., S.K. Cox, and T.B. McKee (1979), "Total Shortwave Radiative Characteristics of Absorbing Finite Clouds," J. Atmos. Sci., 36, 508-518.

Diak, G., C. Gautier, and S. Masse (1982), "An Operational System for Mapping Insolation from GOES Satellite Data," Solar Energy, 28 371-376.

Fritz, S., P. Krishna Rao, and M. Weinstein (1964), "Satellite Measurements of Reflected Solar Energy and the Energy Received at the Ground," J. Atmos. Sci., 21, 141-151.

Fymat, A.L. and V.E. Zuev (1978), Remote Sensing of The Atmosphere: Inversion Methods and Applications, Elsevier Scientific Publishing Co., New York, 1978.

Gautier, C., G. Diak, S. Masse (1980), "A Simple Model to Estimate Incident Solar Radiation at the Surface from GOES Satellite Data," J. of Appl. Meteor. 19, 1005-1012.

Gautier, C. (1982), "Mesoscale Insolation Variability Derived from Satellite Data", J. Appl. Meteor., 21, 51-58.

Green, W.B., P.L. Jepsen, J.E. Krezner, R.M. Ruiz, A.A. Schwartz and J.B. Seidman (1975), "Removal of Instrument Signature from Mariner 9 Television Images of Mars," Appl. Opt., 14.

Gillespie, A.R. and J.M. Soha (1972), "An Orthographic Photomap of the South Pole of Mars from Mariner 7," Icarus, 16, 522-527.

Hanson, K.J. and J.J. DeLuisi (1981), "Forecasting Solar Energy on Synoptic and Longer Time Scales with Mean Values and Persistance Methods," from Satellites and Forecasting of Solar Radiation, Proceedings of First Workshop on Terrestrial Solar Resource Forecasting and on the Use of Satellites for Terrestrial Solar Resource Assessment, Washington, D.C., February 2-5, 1981.

Hanson, K.J., T.H. Vonder Haar, and V.E. Suomi (1967), "Reflection of Sunlight to Space and Absorption by the Earth and Atmosphere Over the United States During Spring 1962," Monthly Weather Review, 95,354-362.

Hay, J. (1980), Department of Geography, University of British Columbia Report to the Department of Energy Insolation Resource Assessment Program, University of California, Davis, 19-21 August.

Hernandez, E. (1977), "On the Numerical Computation of Solar Radiation Parameters from Satellite Cloud Data," World Meteor. Org. No. 477, Solar Energy, 162-170.

Hiser, H.W., and H.V. Senn (1980), "Mesoscale Mapping of Available Solar Energy at the Earth's Surface by Use of Satellites," Solar Energy, 24, 129-141.

Hiser, H.W. (1978), "Use of Satellites in Solar Applications," paper presented at International Symposium-Workshop on Solar Energy, 16-22 June 1978, Cairo, Egypt.

Hulstrom, R.L. (1978). Insolation Models, Data and Algorithms Annual Report FY78. SERI/TR-36-110. December 1978.

Hulstrom, R.L. (1981), "Solar User Needs for Forecasts and Satellite Mapping of Insolation," in Satellites and Forecasting of Solar Radiation, A Workshop of the Solar Radiation Division of American Section of ISES, Washington, D.C., February 2-5, 131-133.

Idso, S. (1970), "The Transmittance of the Atmosphere to Solar Radiation on Individual Clear Days," J. Appl. Meteor., 9,239-241.

Karalis, J.D. (1972), "Precipitable Water and Its Relationship to Surface Dew-point and Vapor Pressure in Athens,", J. Appl. Meteor., 13, 760-766.

Kowalik, W.S. and S.E. Marsh (1982), "A Relation Between Landsat Digital Numbers, Surface Reflectance, and the Cosine of the Solar Zenith Angle," Remote Sensing of Environment, 12, 39-55.

Liou, K.M. (1976), "On the Absorption, Reflection, and Transmission of Solar Radiation in Cloudy Atmospheres," J. Atmos. Sci., 31, 798-805.

Logan, Thomas L., James R. Huning, David L. Glackin (1982). Cloud Cover Typing From Environmental Satellite Imagery. Interim Report. For United States Navy, Naval Environmental Prediction Research Facility, Task 80-1565, Jet Propulsion Laboratory, California Institute of Technology, Pasadena, CA (May).

Lowry, D.A. and H.R. Glahn, 1969, "Relationship Between Integrated Atmospheric Moisture and Surface Weather," J. Appl. Meteor., 8, 762-768.

McCleese, D.J. (1978): "Remote Sensing of Cloud Properties from Nimbus 5," in Remote Sensing of The Atmosphere: Inversion Methods and Applications, by A.L. Fymat and V.E. Zuev, Elsevier Scientific Publishing Co., New York, 295-304.

McLeod, R.G. and H.B. Johnson (1980), "Resource Inventory Techniques Used in the California Desert Conservation Area," Proceedings: Arid Land Resource Inventories Workshop, La Paz, Mexico, November 30-December 6.

Norton, C.C., F.R. Mosher, B. Hinton, D.W. Martin, D. Santek, and W. Kuhlow (1980), "A Model for Calculating Desert Aerosol Turbidity Over the Oceans from Geostationary Satellite Data," J. Appl. Meteor., 19, 633-644.

Paltridge, G.W. (1973), "Direct Measurements of Water Vapor Absorption of Solar Radiation in the Free Atmosphere," J. Atmos. Sci., 30, 156-160.

Paltridge, G.W., and C.M.R. Platt (1976). Radiative Processes in Meteorology and Climatology, Elsevier Scientific Publishing Co., New York.

Preuss, H.J., and J.F. Geleyn (1980), "Surface albedos derived from satellite data and their impact on forecast models," Arch. Met. Geoph. Biokl., Ser. A, 29, 345-356.

Randall, C., B.R. Johnson and M.E. Whitson, Jr. (1980), Measurements of Typical Insolation Variation at Daggett, California - (3 Volumes). Aerospace Report No.1 ATR-80 (7747)-1, The Aerospace Corporation, 1 March.

Randall, C. and M.E. Whitson Jr. (1977), Hourly Insolation and Meteorological Data Bases Including Improved Direct Insolation Estimates. The Aerospace Corporation, December.

Raschke, E., and H.J. Preuss (1979), "The Determination of the Solar Radiation Budget at the Earth's Surface from Satellite Measurements," Meteorologia Research (Moscow), 32, 18-28.

Reid, J.S., J.R. Huning, J.H. Smith (1981), "Solar Radiation Data Requirements for the Engineering Analysis of Solar Thermal Systems," Solar Thermal Test Facilities Users Association (STTFUA), Albuquerque, NM, January 1981.

Reitan, D.H. (1963), "Surface Dew Point and Water Vapor Aloft," J. Appl. Meteor., 14, 776-779.

Reynolds, S.W., and T.H. Vonder Haar and S.K. Cox (1975), "The Effects of Solar Radiation Absorption in the Tropical Atmosphere," J. Appl. Meteor., 14, 433-444.

Reynolds, D.W., T. B. McKee and K.S. Danielson (1978), "Effects of Cloud Size and Cloud Particles on Satellite-Observed Reflected Brightness," J. Atmos. Sci., 35, 160-164.

Rindfleisch, T.C., J.A. Dunne, H.J. Frieden, W.D. Stromberg and R.M. Ruiz (1971), "Digital Processing of the Mariner 6 and 7 Pictures," J. Geophys. Res., 76 (2) 394-417.

Rockwood, A.A., and S.K. Cox (1978), "Satellite Inferred Surface Albedo Over Northwestern Africa," J. Atmos. Sci., 35, 513-522.

Smith, W.L. (1966), "Note on the Relationship Between Total Precipitable Water and Surface Dew Point," J. Appl. Meteor., 5, 727-727.

Soha, J.M., D.J. Lynn, J.J. Lorre, J.A. Mosher, N.N. Thayer, D.A. Elliott, W.D. Benton and R.E. Dewar (1975), "IPL Processing of the Mariner 10 Images of Mercury," J. Geophys. Res., 80, 17.

Staton, C. (1982), NOAA/NESS, personal communication, August 31, 1982.

Stephens, G.L. (1978), "Radiation Profiles in Extended Water Clouds, Parts I and II, Theory and Parameterization Schemes," J. Atmospheric Sci., 35, 2111-2132.

Stephens, G.L., G.W. Paltridge, and C.M.R. Platt (1978), "Radiation Profiles in Extended Water Clouds, III: Observations," J. Atmos. Sci., 35, 2133-2141.

Stigter, C.J., "Sampling and Estimating of Better Defined Cloudiness for Dar es Salaam" (1982), Solar Energy 28, 1, 49-53.

Sutherland, R.A., J.L. Langford, J.F. Bartholic, and R.G. Bill (1978), "A Real-Time Satellite Data Acquisition, Analysis and Display System - A Practical Application of the GOES Network," J. Appl. Meteor., 18, 355-360.

Tarpley, J.D. (1979), "Estimating Incident Solar Radiation at the Surface from Geostationary Satellite Data," J. Appl. Meteor., 18, 1172-1181.

Tarpley, Dan J., Stanley R. Schneider, J. Emmett Bragg, and Marshall P. Waters, III (1978), "Satellite Data Set for Solar Incoming Radiation Studies," NOAA Technical Memorandum 96.

Twomey, S. (1970), "On the Possible Absorption of Visible Light by Clouds," J. Atmos. Sci., 27, 514-515.

Twomey, S. (1976), "Computations of the Absorption of Solar Radiation by Clouds," J. Atmos. Sci., 33, 1087-1901.

Twomey, S. (1978), "Comments on Effects of Cloud Size and Cloud Particles on Satellite-Observed Reflected Brightness," J. Atmos. Sci., 35, 2389-2391.

Viswanadham, Y. (1981), "The Relationship Between Total Precipitable Water and Surface Dew Point," J. Appl. Meteor., 20, 3-20.

Vonder Harr, T.H. and J.S. Ellis (1978), "Determination of the Solar Energy Microclimate of the United States Using Satellite Data," Final Report, NAS5-22372, July, 68pp.

Willand, J.H. and M. Tubman (1979), "Objective Cloud Analysis from Satellite Infrared and Visible Digital Data," Final Report ERT Document No. P-3355-F, September, 63 pp. (excluding Appendix).

Yamamoto, G. (1962), "Direct Absorption of Solar Radiation by Atmospheric Water Vapor, Carbon Dioxide and Molecular Oxygen," J. Atmos. Sci., 19, 182-188.

Yinger, R.J. (1982), "The West Associates Solar Resource Evaluation Project," Sponsored by West Associates, Southern California Edison, Research and Development, 82-RD-4, 183 pp.

Zobrist, A.L., "Multiple Frame, Full Resolution Landsat Mosaicking to Standard Map Projection," Proceedings of the American Society of Photogrammetry, Fall Technical Meeting, October 15-20, 1978 Albuquerque, N.M., 608-616.
Zobrist, A.L. and N.A. Bryant, "Map Characteristics of Landsat Mosaics", Proceedings of the American Society of Photogrammetry, 45th Annual Meeting, March 18-24, 1979, Washington, D.C., Vol. I, 260-273.

Zobrist, A.L., N.A. Bryant, S.Z. Friedman, G.L. Angelici (1978), Image Based Information System (IBIS) System Guide, JPL Publication 900-909. (Available from COSMIC).

APPENDIX A

VICAR/IBIS

INFORMATION SYSTEM TECHNOLOGY

APPENDIX A

VICAR/IBIS
INFORMATION SYSTEM TECHNOLOGY

I.0 BACKGROUND

Computer image processing at Caltech's Jet Propulsion Laboratory began almost two decades ago with computer processing of imagery returned by Ranger and Surveyor spacecraft. The trend at the JPL Image Processing Laboratory has been toward increasingly complex processing of digital imagery, and more recently toward integration of remotely sensed imagery with non-imaging data bases. The early processing performed on planetary imaging generally involved processing of single images acquired in a single spectral band. The processing ranged from simple enhancement of an individual image to more complex processing including removal of camera system distortions and cartographic projection (e.g., Green, et al., 1975; Soha, et al., 1975; Gillespie and Soha, 1972). It was in this computer environment that the Image Based Information System (IBIS) was developed as a subset of the overall JPL Video Image Communication and Retrieval (VICAR) image processing system in 1976 (Bryant and Zobrist, 1976). The image raster approach used in the Image Based Information System (IBIS) became possible as the state-of-the-art in image file handling became efficient, and continuous surface geometric rectification software was developed.

The initial motivation for development of the Image Based Information System (IBIS) was to permit the processing of a Landsat thematic map showing land use or land cover in conjunction with a census tract polygon file to produce a tabulation of land use acreages per census tract. An analysis of the steps necessary to achieve this basic capability brought forth two facts. First, a large number of image processing and data manipulation capabilities

would be needed for even the simplest case. Second, with proper design, the minimal system can be extended into a general information system with novel features and capabilities. The term Image Based Information System was adopted because the image data type and image processing operations are crucial to many of the new capabilities.

Digital image processing techniques can be applied to interface existing geocoded data sets and information management systems with thematic maps and remotely sensed imagery. The basic premise is that geocoded data sets can be referenced to a raster scan that is equivalent to an ultrafine mesh grid cell data set, and that images taken of thematic maps or from remote sensing platforms can be converted to a raster scan. Until recently, the image format has been used primarily as a computer processable equivalent of a photograph, with the value stored in each cell of the image representing a shade of gray or a color. But if the image is of a geographical point it can be accessed immediately by position in the image matrix. From these initial assumptions, there has developed a variety of applications which range from simple tabulations to complex inventories, modelling, and the system's incorporation as the essential spatial data management system for achieving multiple-frame digital mosaics and Landsat image map projections (Zobrist, 1978).

2.0 DATA CAPTURE AND STORAGE

IBIS is a raster-based information system. Most data entered into IBIS will be in raster (image based) format. However, the system is configured in a manner that other data types such as graphical and tabular data may be used in analysis as well.

For each data type to be included, the primary consideration is data entry, for it is this process where the greatest costs and difficulties are usually incurred. Data input can be represented as three-stage process:

RAW DATA

(1) DATA CAPTURE

EDITING

COMPUTER COMPATIBLE DATA

(2) Reformating

INITIAL DATA BASE

(3) Obtain Temporal Baseline

WORKING DATA BASE

The first stage, Data Capture, includes all operations up to the point where a data file is computer readable. Data capture costs are extremely high for many basic kinds of data.

GOES imagery is a particularly attractive data source because it is already computer compatible and gives up-to-date coverage of large areas at nominal cost. Editing costs vary widely depending upon the nature of the data source. Reformatting can also be a major operation where large data files are involved. An example occurs when data are gathered by various districtings (e.g., county, census tract) but must be reformatted to a common districting so that analysis can be performed. The final stage of data input is to obtain a temporal baseline, which in the cloud cover mapping case can be an arbitrary selection based on available ground station data.

The image formatted Data Plane is the primary data type utilized in IBIS processing. IBIS data planes may be obtained directly in image form, as in GOES imagery, or they may be derived from data compiled by sources such as the U.S. Geological Survey, the U.S. Bureau of the Census, and the Defense

Mapping Agency. Regardless of data type and origin, all data planes are incorporated into a data set which is referred to as the IBIS Data Base. When investigating a specific problem, a data plane may be included in, excluded from, or modified before any IBIS processing step. New data planes may be constructed with the system and may be used in subsequent processing steps. In order to maintain geometric consistency between all data planes included in the data base, an image plane exhibiting good radiometric or planimetric qualities is designated to be the Planimetric Base. All other data planes are geometrically corrected to allow registration to the planimetric base.

The user of IBIS can integrate various data types to form an IBIS data base. Since the primary data structure is a raster format, image data planes are directly entered into the system. Graphical forms of data, usually obtained in cartesian reference form, must be transformed into image space prior to inclusion as a data plane. Tabular data are not transformed into image space, but are linked to the image data base through a logical interface. Data processing requirements for each data type are unique and will be covered individually.

2.1 Image Data

Historically, most image data sets entered into the data base have usually been derived from LANDSAT imagery or other multispectral scanner sources such as GOES. Other data are digitally encoded or scanned from photographic products. Since image data planes are not always derived from the same source, there may be no common spatial alignment between them. Consequently, provisions have been made to register these data sets in order to obtain a unified spatial surface. The nonaligned data must undergo resampling and "rubber-sheeting" procedures. Geometric correction procedures and spatial

rectification routines for modifying image data are features of the VICAR image processing system. Although not specifically considered to be IBIS programs, these and other VICAR programs are necessary parts of the IBIS process. VICAR software is often used to obtain special information from image data sources. Multispectral classification of Landsat imagery is one example of a VICAR procedure which produces a data set used in IBIS procedures.

2.2 Vector

Vector data (also known as polygonal or graphics data) may also be entered into the IBIS data base. Vector data are either produced locally on a coordinate digitizer or are obtained from data tape. Regardless of data origin, vector data are transformed into image space prior to inclusion in the IBIS data base.

As with image data, vector data files must be in registry with the primary data base. Provisions have been made within IBIS to achieve the proper geometric corrections. (These corrections are made before the data are transformed into image space).

The registration technique utilized is a two-step process. Initially, a general surface fit is achieved through the use of a least squares affine transformation. Then, an exact geometric correspondence is obtained by implementing a "rubber-sheeting" procedure. The deformation of the original surface is controlled by the selection of tiepoints linking geographical features which are identifiable on both the vector data file and the primary data base.

Point and vector data are transformed into image space after geometric modifications are completed. Three dimensional or z-value data (x, y, z) are processed in a similar manner. The cartesian reference components of the data

(x, y) are transformed into image space coordinate values, while the z-value remains unchanged.

2.3 Tabular Data

Tabular data may be entered into IBIS via computer cards or digital tape. These data are stored in a tabular file that is linked to the data base through a logical interface. As a result of this link, such data files are termed interface files.

One of the more important graphical data files entered onto the IBIS data base is the Geo-reference Plane. The georeference plane is a polygon file which is used in data aggregation and map generation procedures. Once the geo-reference plane is transformed into image space, each polygon, or region, must be identified. The region identification process involves the assignment of a unique value (or gray tone) to each individual region. After region identification, the geo-reference plane may be used in several higher order IBIS procedures. For example, polygon overlay of the geo-reference plane with some other image data plane can be initiated. Or, the gray values of each polygon in the geo-reference base may be modified to produce a map depicting the results of a modelling application with data stored in an interface file. Several geo-reference planes may be included in an IBIS data base. The maximum number of regions that can be included in one geo-reference plane is virtually unlimited. Currently, up to 20,000 regions can be identified by gray value for an individual geo-reference plane.

All tabular files (interface files) are linked to at least one of the geo-reference planes included in the IBIS data base. The specific link is obtained by storing the numerical value (gray tone) representing each region of the geo-reference plane with tabular data describing attributes of that

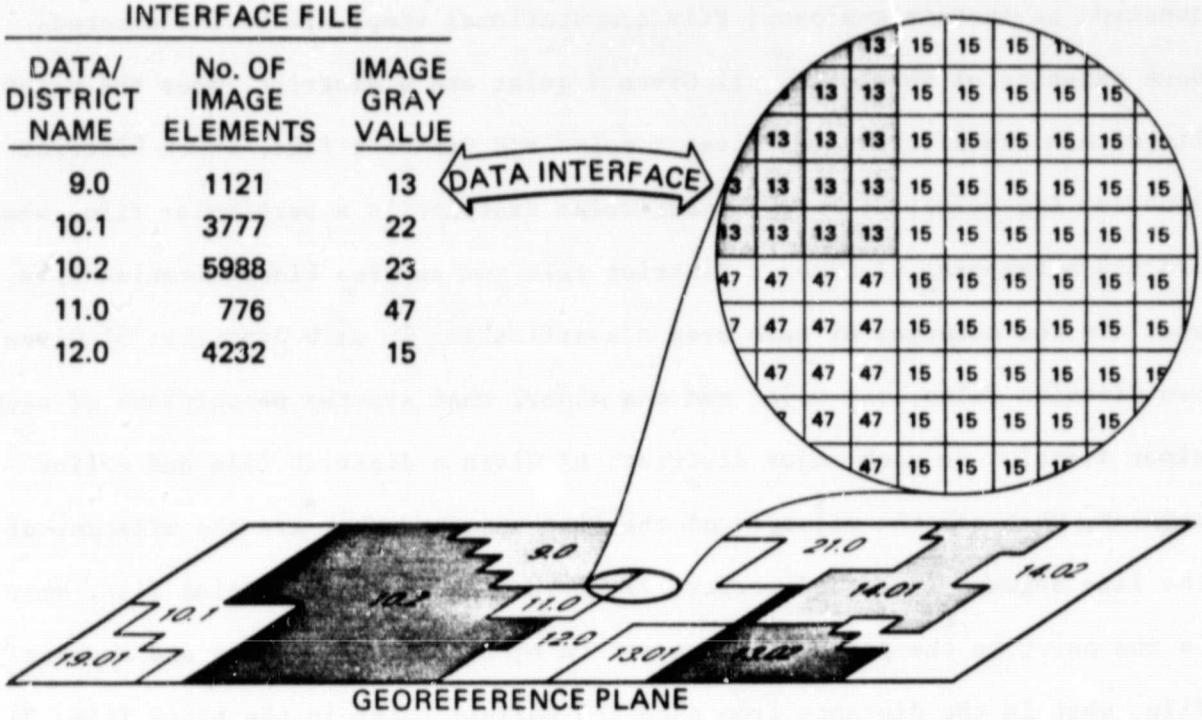

Figure A-1. The Data Interface

region (Figure A-1). Attribute data may be statistical in origin, an identification code, or may be the result of an image plane comparison routine such as polygon overlay or cross-tabulation.

3.0 QUERY AND RETRIEVAL

Once a working data base is established, provisions must be made for information retrieval, information analysis, and report generation. Operations here are usually of a much smaller scale than data capture in terms of time and cost, but there is a question of flexibility, ease of use, and system cost. All data analyses can be laid out as a sequence of primitive steps, thus, a functional requirement is that an adequate set of primitive operations

can be implemented. Mathematical and statistical analyses of tabular files are well-understood, and packaged systems can easily be interfaced. The open question is whether geo-based file computational steps can be implemented. Some examples of these are: 1) Given a point and a district, does the point lie within the district; 2) Given a point and district file, which district contains the point; 3) Given a particular district in a particular file, what are its neighbors; 4) Given a district file and an area classification file, what are the acreages of each area classification in each district; 5) Given two district files, one major and one minor, what are the proportions of each minor district in each major district; 6) Given a district file and a line segment, what are the mileages of the line segment, what are the mileages of the line segment in each district; 7) Given a point p and a point file, what is the point in the point file nearest to p; 8) Given a point p and a point file, what is the distance from p to the nearest point in the point file; 9) Given a point and a line segment file, which line segment passes closest to the point; 10) Given a density map and a district file, what are the volumes in each district (spatial integral of density); 11) Given a district, what is the centermost point (an inside point which is farthest from the boundary).

The preceding list is just a sample of the spatial or geometric calculations which need to be performed by a comprehensive geo-base information system. More complex operations will usually be implemented as a sequence of these primitive operations, but because of the magnitude of the data files and because of iteration due to modelling, computation time can be a serious problem. A method which solves one of the primitive problems in 0.1 second may seem usable, but not if it has to be performed ten million times for a particular application.

It is worth noting here that many of these operations are difficult and time consuming if the working data base is in vector format (i.e., lines are specified by their end points and a district is given by a sequence of line segments). In particular, the operation called polygon overlay, which solves primitive problems four and five, is extremely difficult to perform on large files in vector format.

Logical and mathematical interfaces have been provided to link all data files in an IBIS data base superstructure (Figure A-2). By utilizing these interfaces, information may be derived from simple associations, or comparisons between two or more data files stored in an IBIS data base.

Procedures for data output and data manipulation have been derived as part of the Image Based Information System. Maps may be generated and tabular reports can be obtained.

Data stored in either the data base or an interface file can be modified or maniuplated with IBIS software. New data planes and interface files are easily generated. Four basic data manipulation procedures are currently available:

3.1 Data Manipulation Between Image Planes

New image data planes are generated as a function of two or more image data planes. Chiefly, procedures implemented to derive such data planes are VICAR routines, although some IBIS routines are also used. Simple transformations such as image addition, subtraction, multiplication, and division are easily obtained. Complex functions are handled nearly as easily, and precise mathematical formulas may be specified. Image enhancement routines are available, as are several data classification and stratification routines.

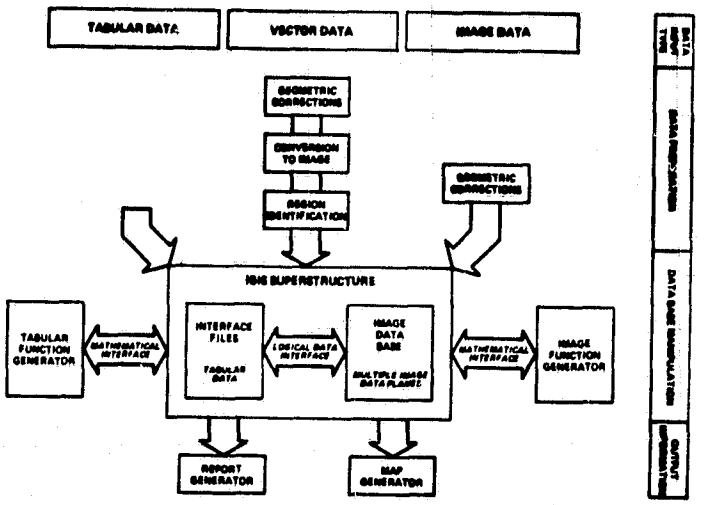

Figure A-2. A Configuration Diagram of the Image Based Information System

3.2 Data Manipulation Within the Interface File

Most functions available in the image domain are also available for analysis of a tabular data. Resultant from such operations, new tabular data entries are generated. Complex mathematical functions may be used to derive higher order properties of data stored in an interface file.

3.3 Data Manipulation of Image Data Into Tabular Data

By implementing certain IBIS routines, data originally stored in image format may be summarized and copied into a tabular file. The majority

of these routines are aggregated functions, an example of which is histogram generation. IBIS procedures for polygon overlay and cross-tabulation are within this realm of data transfer programs.

3.4 Data Manipulation of Tabular Data Into Image Data

The representation of tabular data in image form is primarily used as an output aid. By the implementation of a map-generating routine, any geo-reference base can be modified as a function of an interface file. Modelling of data is performed similarly. Data planes produced in this manner can be entered into the IBIS data base for subsequent operations.

APPENDIX B

SAMPLE PRINT-OUTS: CLOUD STATISTICS

3 APRIL 1980 2245 GMT

SOUTHERN CALIFORNIA CLOUD/SHADOW MAPPING FROM GOES VS DATA
PROJECT 70-1400 JET PROPULSION LABORATORY, PASADENA, CALIF

GRID CELL	PHYSIO REGION	PHYSI NUM	FILE SEQ	SENSOR & DATE	TIME GMT	CELL SQ KM	% AREA CLOUD	% AREA SHADOW	% CLOUD OPAQUE	% SHAD OPAQUE	% BAD DATA
370	EMJ1	1	58	2480094	2245	208	0	0	0	0	0
371	EMJ1	1	58	2480094	2245	208	0	0	0	0	0
372	EMJ1	1	58	2480094	2245	208	0	0	0	0	0
373	EMJ1	1	58	2480094	2245	208	0	0	0	0	0
374	EMJ1	1	58	2480094	2245	208	0	6	0	25	0
375	EMJ1	1	58	2480094	2245	208	0	6	0	25	0
376	EMJ1	1	58	2480094	2245	208	0	6	0	29	0
377	EMJ1	1	58	2480094	2245	208	0	0	0	0	0
378	EMJ1	1	58	2480094	2245	208	0	0	0	0	0
379	EMJ1	1	58	2480094	2245	208	0	6	0	29	0
380	EMJ1	1	58	2480094	2245	208	0	0	0	0	0
381	EMJ1	1	58	2480094	2245	208	0	13	0	29	0
382	EMJ1	1	58	2480094	2245	208	0	0	0	0	0
385	EMJ1	1	58	2480094	2245	208	0	19	0	26	0
386	EMJ1	1	58	2480094	2245	208	0	13	0	31	0
387	EMJ1	1	58	2480094	2245	208	6	0	25	0	0
388	EMJ1	1	58	2480094	2245	208	9	0	0	0	0
389	EMJ1	1	58	2480094	2245	208	44	0	51	0	0
390	EMJ1	1	58	2480094	2245	208	6	13	25	31	0
391	EMJ1	1	58	2480094	2245	208	25	0	28	0	0
392	EMJ1	1	58	2480094	2245	208	25	0	35	0	0
393	EMJ1	1	58	2480094	2245	208	38	6	47	33	0
394	EMJ1	1	58	2480094	2245	208	0	6	0	46	0
405	EMJ1	1	58	2480094	2245	208	6	6	25	25	0
407	EMJ1	1	58	2480094	2245	208	0	0	0	0	0
408	EMJ1	1	58	2480094	2245	208	0	0	0	0	0
409	EMJ1	1	58	2480094	2245	208	0	0	0	0	0
410	EMJ1	1	58	2480094	2245	208	0	25	0	29	0
411	EMJ1	1	58	2480094	2245	208	0	6	0	25	0
412	EMJ1	1	58	2480094	2245	208	0	0	0	0	0
413	EMJ1	1	58	2480094	2245	208	0	0	0	0	0
416	EMJ1	1	58	2480094	2245	208	0	6	0	25	0
418	EMJ1	1	58	2480094	2245	208	0	13	0	25	0
419	EMJ1	1	58	2480094	2245	208	0	6	0	29	0
420	EMJ1	1	58	2480094	2245	208	0	0	0	0	0
421	EMJ1	1	58	2480094	2245	208	0	0	0	0	0
424	EMJ1	1	58	2480094	2245	208	0	0	0	0	0
425	EMJ1	1	58	2480094	2245	208	0	6	0	63	0
426	EMJ1	1	58	2480094	2245	208	0	6	0	33	0
427	EMJ1	1	58	2480094	2245	208	0	6	0	33	0
441	EMJ1	1	58	2480094	2245	208	0	0	0	0	0
442	EMJ1	1	58	2480094	2245	208	0	0	0	0	0
443	EMJ1	1	58	2480094	2245	208	0	0	0	0	0
444	EMJ1	1	58	2480094	2245	208	0	6	0	33	0
445	EMJ1	1	58	2480094	2245	208	0	0	0	0	0
446	EMJ1	1	58	2480094	2245	208	0	0	0	0	0
447	EMJ1	1	58	2480094	2245	208	0	0	0	0	0
452	EMJ1	1	58	2480094	2245	208	0	6	0	25	0

SOUTHERN CALIFORNIA CLOUD/SHADOW MAPPING FROM GOES VS DATA
PROJECT 73-1453 JET PROPULSION LABORATORY, PASADENA, CALIF

GRID CELL	PHYSIO REGION	PHYSI NUMB	FILE SEQ	SENSOR & DATE	TIME GMT	CELL SQ KM	% AREA CLOUD	% AREA SHADOW	% CLOUD OPAQUE	% SHAD OPAQUE	% BAD DATA
453	EMJ1	1	58	2480094	2245	208	0	0	0	0	0
454	EMJ1	1	58	2480094	2245	208	0	0	0	0	0
455	EMJ1	1	58	2480094	2245	208	0	0	0	0	0
459	EMJ1	1	58	2480094	2245	208	0	0	0	0	0
460	EMJ1	1	58	2480094	2245	208	0	0	0	0	0
475	EMJ1	1	58	2480094	2245	208	0	0	0	0	0
476	EMJ1	1	58	2480094	2245	208	0	0	0	0	0
477	EMJ1	1	58	2480094	2245	208	0	0	0	0	0
478	EMJ1	1	58	2480094	2245	208	0	0	0	0	0
479	EMJ1	1	58	2480094	2245	208	0	0	0	0	0
480	EMJ1	1	58	2480094	2245	208	0	0	0	0	0
481	EMJ1	1	58	2480094	2245	208	0	0	0	0	0
482	EMJ1	1	58	2480094	2245	208	0	0	0	0	0
483	EMJ1	1	58	2480094	2245	208	0	6	0	25	0
485	EMJ1	1	58	2480094	2245	208	0	0	0	0	0
488	EMJ1	1	58	2480094	2245	208	0	0	0	0	0
493	EMJ1	1	58	2480094	2245	208	0	0	0	0	0
509	EMJ1	1	58	2480094	2245	208	0	13	0	25	0
510	EMJ1	1	58	2480094	2245	208	0	0	0	0	0
511	EMJ1	1	58	2480094	2245	208	0	6	0	25	0
512	EMJ1	1	58	2480094	2245	208	0	0	0	0	0
513	EMJ1	1	58	2480094	2245	208	0	0	0	0	0
514	EMJ1	1	58	2480094	2245	208	0	0	0	0	0
515	EMJ1	1	58	2480094	2245	208	0	0	0	0	0
516	EMJ1	1	58	2480094	2245	208	0	0	0	0	0
517	EMJ1	1	58	2480094	2245	208	0	6	0	25	0
518	EMJ1	1	58	2480094	2245	208	0	6	0	25	0
521	EMJ1	1	58	2480094	2245	208	0	0	0	0	0
542	EMJ1	1	58	2480094	2245	208	0	0	0	0	0
543	EMJ1	1	58	2480094	2245	208	0	13	0	25	0
544	EMJ1	1	58	2480094	2245	208	0	6	0	29	0
545	EMJ1	1	58	2480094	2245	208	0	0	0	0	0
546	EMJ1	1	58	2480094	2245	208	0	0	0	0	0
547	EMJ1	1	58	2480094	2245	208	0	0	0	0	0
548	EMJ1	1	58	2480094	2245	208	0	0	0	0	0
549	EMJ1	1	58	2480094	2245	208	0	6	0	29	0
550	EMJ1	1	58	2480094	2245	208	0	0	0	0	0
553	EMJ1	1	58	2480094	2245	208	0	0	0	0	0
554	EMJ1	1	58	2480094	2245	208	0	0	0	0	0
575	EMJ1	1	58	2480094	2245	208	0	0	0	0	0
576	EMJ1	1	58	2480094	2245	208	6	0	25	0	0
577	EMJ1	1	58	2480094	2245	208	0	6	0	29	0
578	EMJ1	1	58	2480094	2245	208	0	6	0	25	0
579	EMJ1	1	58	2480094	2245	208	0	0	0	0	0
580	EMJ1	1	58	2480094	2245	208	0	0	0	0	0
581	EMJ1	1	58	2480094	2245	208	0	0	0	0	0
582	EMJ1	1	58	2480094	2245	208	0	0	0	0	0
583	EMJ1	1	58	2480094	2245	208	0	0	0	0	0

ORIGINAL PAGE IS
OF POOR QUALITY

SOUTHERN CALIFORNIA CLOUD/SHADOW MAPPING FROM GOES VS DATA
PROJECT 73-1650 JET PROPULSION LABORATORY, PASADENA, CALIF

GRID CELL	PHYSIO REGION	PHYSI NUMB	FILE SEQ	SENSOR & DATE	TIME GMT	CELL SQ KM	% AREA CLOUD	% AREA SHADOW	% CLOUD OPAQUE	% SHAD OPAQUE	% BAD DATA
587	EMJ1	1	58	2480094	2245	208	0	0	0	0	0
609	EMJ1	1	58	2480094	2245	208	0	0	0	0	0
610	EMJ1	1	58	2480094	2245	208	0	0	0	0	0
611	EMJ1	1	58	2480094	2245	208	0	6	0	29	0
612	EMJ1	1	58	2480094	2245	208	6	0	25	0	0
613	EMJ1	1	58	2480094	2245	208	0	0	0	0	0
614	EMJ1	1	58	2480094	2245	208	0	0	0	0	0
615	EMJ1	1	58	2480094	2245	208	0	0	0	0	0
618	EMJ1	1	58	2480094	2245	208	0	0	0	0	0
619	EMJ1	1	58	2480094	2245	208	0	6	0	25	0
620	EMJ1	1	58	2480094	2245	208	0	0	0	0	0
642	EMJ1	1	58	2480094	2245	208	0	0	0	0	0
643	EMJ1	1	58	2480094	2245	208	0	0	0	0	0
644	EMJ1	1	58	2480094	2245	208	0	6	0	25	0
645	EMJ1	1	58	2480094	2245	208	0	0	0	0	0
646	EMJ1	1	58	2480094	2245	208	0	0	0	0	0
647	EMJ1	1	58	2480094	2245	208	0	0	0	0	0
648	EMJ1	1	58	2480094	2245	208	0	0	0	0	0
649	EMJ1	1	58	2480094	2245	208	0	6	0	29	0
650	EMJ1	1	58	2480094	2245	208	0	6	0	25	0
651	EMJ1	1	58	2480094	2245	208	0	0	0	0	0
652	EMJ1	1	58	2480094	2245	208	0	0	0	0	0
653	EMJ1	1	58	2480094	2245	208	0	0	0	0	0
654	EMJ1	1	58	2480094	2245	208	0	19	0	28	0
675	EMJ1	1	58	2480094	2245	208	0	6	0	25	0
676	EMJ1	1	58	2480094	2245	208	0	0	0	0	0
677	EMJ1	1	58	2480094	2245	208	0	0	0	0	0
678	EMJ1	1	58	2480094	2245	208	0	6	0	25	0
679	EMJ1	1	58	2480094	2245	208	0	19	0	26	0
680	EMJ1	1	58	2480094	2245	208	0	6	0	25	0
681	EMJ1	1	58	2480094	2245	208	0	0	0	0	0
682	EMJ1	1	58	2480094	2245	208	0	0	0	0	0
683	EMJ1	1	58	2480094	2245	208	0	13	0	27	0
684	EMJ1	1	58	2480094	2245	208	0	6	0	25	0
685	EMJ1	1	58	2480094	2245	208	0	6	0	25	0
686	EMJ1	1	58	2480094	2245	208	0	6	0	25	0
687	EMJ1	1	58	2480094	2245	208	0	6	0	25	0
710	EMJ1	1	58	2480094	2245	208	0	6	0	25	0
711	EMJ1	1	58	2480094	2245	208	0	13	0	25	0
712	EMJ1	1	58	2480094	2245	208	0	6	0	25	0
713	EMJ1	1	58	2480094	2245	208	0	6	0	29	0
714	EMJ1	1	58	2480094	2245	208	0	6	0	25	0
715	EMJ1	1	58	2480094	2245	208	0	0	0	0	0
716	EMJ1	1	58	2480094	2245	208	0	19	0	28	0
717	EMJ1	1	58	2480094	2245	208	0	13	0	27	0
718	EMJ1	1	58	2480094	2245	208	0	6	0	25	0
719	EMJ1	1	58	2480094	2245	208	0	6	0	29	0
720	EMJ1	1	58	2480094	2245	208	0	19	0	28	0

SOUTHERN CALIFORNIA CLOUD/SHADOW MAPPING FROM GOES VS DATA
PROJECT 78-1450 JET PROPULSION LABORATORY, PASADENA, CALIF

GRID CELL	PHYSIO REGION	PHYSI NUM	FILE SEQ	SENSOR & DATE	TIME GMT	CELL SQ KM	% AREA CLOUD	% AREA SHADOW	% CLOUD OPAQUE	% SHAD OPAQUE	% BAD DATA
315	4743	2N2	558	24803094	2N2	104	1	28	3	29	0
316	4743		558	24803094	2N2	104					
317	4743		558	24803094	2N2	104					
10317						*1522					

ORIGINAL PAGE IS
OF POOR QUALITY

SOUTHERN CALIFORNIA CLOUD/SHADOW MAPPING FROM GOES VS DATA
PROJECT 70-1450 JET PROPULSION LABORATORY, PASADENA, CALIF

GRID CELL	PHYSIO REGION	PHYSI NUMB	FILE SEQ	SENSOR & DATE	TIME GMT	CELL SQ KM	% AREA CLOUD	% AREA SHADOW	% CLOUD OPAQUE	% SHAD OPAQUE	% NO DATA
						14173					
47	RIVY	5	58	2480094	2245	832	3	0	27	0	0
64	RIVY	5	58	2480094	2245	832	0	8	0	25	0
65	RIVY	5	58	2480094	2245	832	0	2	0	25	0
81	RIVY	5	58	2480094	2245	832	0	5	0	25	0
82	RIVY	5	58	2480094	2245	832	2	0	25	0	0
98	RIVY	5	58	2480094	2245	832	0	8	0	26	0
99	RIVY	5	58	2480094	2245	832	0	5	0	25	0
115	RIVY	5	58	2480094	2245	832	0	2	0	25	0
133	RIVY	5	58	2480094	2245	832	0	5	0	26	0
150	RIVY	5	58	2480094	2245	832	0	2	0	25	0
422	RIVY	5	58	2480094	2245	208	0	0	0	0	0
423	RIVY	5	58	2480094	2245	208	0	0	0	0	0
455	RIVY	5	58	2480094	2245	208	0	6	0	25	0
459	RIVY	5	58	2480094	2245	208	0	0	0	0	0
492	RIVY	5	58	2480094	2245	208	0	0	0	0	0
522	RIVY	5	58	2480094	2245	208	0	0	0	0	0
555	RIVY	5	58	2480094	2245	208	0	6	0	29	0
588	RIVY	5	58	2480094	2245	208	0	0	0	0	0
722	RIVY	5	58	2480094	2245	208	0	0	0	0	0
755	RIVY	5	58	2480094	2245	208	0	0	0	0	0
2436	RIVY	5	58	2480094	2245	52	0	0	0	0	0
2834	RIVY	5	58	2480094	2245	52	0	0	0	0	0
2900	RIVY	5	58	2480094	2245	52	0	0	0	0	0
9774	RIVY	5	58	2480094	2245	13	0	0	0	0	0
9905	RIVY	5	58	2480094	2245	13	0	0	0	0	0
						10582					
486	MTN4	6	58	2480094	2245	208	0	6	0	33	0
487	MTN4	6	58	2480094	2245	208	0	0	0	0	0
519	MTN4	6	58	2480094	2245	208	0	0	0	0	0
520	MTN4	6	58	2480094	2245	208	0	6	0	29	0
551	MTN4	6	58	2480094	2245	208	0	0	0	0	0
552	MTN4	6	58	2480094	2245	208	0	6	0	25	0
584	MTN4	5	58	2480094	2245	208	0	0	0	0	0
585	MTN4	6	58	2480094	2245	208	0	13	0	25	0
586	MTN4	6	58	2480094	2245	208	0	0	0	0	0
616	MTN4	6	58	2480094	2245	208	0	6	0	25	0
617	MTN4	6	58	2480094	2245	208	0	6	0	25	0
						2288					
88	MTN2	7	58	2480094	2245	832	6	0	56	0	0
631	MTN2	7	58	2480094	2245	104	0	0	0	0	0
664	MTN2	7	58	2480094	2245	104	25	0	25	0	0

SOUTHERN CALIFORNIA CLOUD/SHADOW MAPPING FROM GOES VS DATA
PROJECT 79-1990 JET PROPULSION LABORATORY, PASADENA, CALIF

GRID CELL	PHYSIC REGION	PHYSIC NUMB	FILE SEQ	SENSOR & DATE	TIME GMT	CELL SQ KM	% AREA CLOUD	% AREA SHADOW	% CLOUD OPAQUE	% SHAD OPAQUE	% BAD DATA
						13	0	0	0	0	0
						13	100	0	25	0	0
						10473	100	0	25	0	0
16266	MTN2	77	556	2224 0094	2245	52	25	0	25	0	0
16553	MTN2	77	556	2224 0094	2245	52	50	0	25	0	0
16661	MTN2	77	556	2224 0094	2245	52	100	0	25	0	0

SOUTHERN CALIFORNIA CLOUD/SHADOW MAPPING FROM GOES VS DATA
PROJECT 70-1400 JET PROPULSION LABORATORY, PASADENA, CALIF

GRID CELL	PHYSIC REGION	PHYSI NUMB	FILE SEQ	SENSOR DATE	TIME GMT	CELL SQ KM	% AREA CLOUD	% AREA SHADOW	% CLOUD OPAQUE	% SHAD OPAQUE	% BAD DATA
10467	CLR	999	566	2480394	2245	13	100	000	33	000	000
10468	CLR	999	566	2480394	2245	13	100	000	38	000	000

SOUTHERN CALIFORNIA CLOUD/SHADOW MAPPING FROM GOES VS DATA
PROJECT 73-1450 JET PROPULSION LABORATORY, PASADENA, CALIF

GRID CELL	PHYSIC REGION	PHYSI NUMB	FILE SEQ	SENSOR & DATE	TIME GMT	CELL SQ KM	% AREA CLOUD	% AREA SHADOW	% CLOUD OPAQUE	% SHAD OPAQUE	% BAD DATA
12575	CDS1	10	58	2480094	2245	13	100	0	42	0	0
12576	CDS1	10	58	2480094	2245	13	0	0	0	0	0
12696	CDS1	10	58	2480094	2245	13	100	0	58	0	0
12697	CDS1	10	58	2480094	2245	13	100	0	58	0	0
12698	CDS1	10	58	2480094	2245	13	100	0	58	0	0
12699	CDS1	10	58	2480094	2245	13	100	0	54	0	0
12700	CDS1	10	58	2480094	2245	13	100	0	58	0	0
12701	CDS1	10	58	2480094	2245	13	100	0	54	0	0
12702	CDS1	10	58	2480094	2245	13	100	0	42	0	0
12703	CDS1	10	58	2480094	2245	13	100	0	46	0	0
12704	CDS1	10	58	2480094	2245	13	100	0	54	0	0
12705	CDS1	10	58	2480094	2245	13	100	0	46	0	0
12706	CDS1	10	58	2480094	2245	13	100	0	46	0	0
12707	CDS1	10	58	2480094	2245	13	100	0	46	0	0
12708	CDS1	10	58	2480094	2245	13	100	0	50	0	0
12709	CDS1	10	58	2480094	2245	13	100	0	38	0	0
12829	CDS1	10	58	2480094	2245	13	100	0	46	0	0
12830	CDS1	10	58	2480094	2245	13	100	0	38	0	0
12831	CDS1	10	58	2480094	2245	13	100	0	38	0	0
12832	CDS1	10	58	2480094	2245	13	100	0	42	0	0
12833	CDS1	10	58	2480094	2245	13	100	0	42	0	0
12834	CDS1	10	58	2480094	2245	13	100	0	42	0	0
12835	CDS1	10	58	2480094	2245	13	100	0	38	0	0
12836	CDS1	10	58	2480094	2245	13	100	0	42	0	0
12837	CDS1	10	58	2480094	2245	13	100	0	38	0	0
12838	CDS1	10	58	2480094	2245	13	100	0	38	0	0
12839	CDS1	10	58	2480094	2245	13	100	0	39	0	0
12840	CDS1	10	58	2480094	2245	13	100	0	42	0	0
12841	CDS1	10	58	2480094	2245	13	0	0	0	0	0
12842	CDS1	10	58	2480094	2245	13	0	0	0	0	0
12843	CDS1	10	58	2480094	2245	13	0	0	0	0	0
12961	CDS1	10	58	2480094	2245	13	100	0	50	0	0
12962	CDS1	10	58	2480094	2245	13	100	0	54	0	0
12963	CDS1	10	58	2480094	2245	13	100	0	46	0	0
12964	CDS1	10	58	2480094	2245	13	100	0	50	0	0
12965	CDS1	10	58	2480094	2245	13	100	0	63	0	0
12966	CDS1	10	58	2480094	2245	13	100	0	54	0	0
12967	CDS1	10	58	2480094	2245	13	100	0	58	0	0
12968	CDS1	10	58	2480094	2245	13	100	0	54	0	0
12969	CDS1	10	58	2480094	2245	13	100	0	58	0	0
12970	CDS1	10	58	2480094	2245	13	100	0	50	0	0
12971	CDS1	10	58	2480094	2245	13	100	0	50	0	0
12972	CDS1	10	58	2480094	2245	13	100	0	63	0	0
12973	CDS1	10	58	2480094	2245	13	100	0	58	0	0
12974	CDS1	10	58	2480094	2245	13	100	0	33	0	0
12975	CDS1	10	58	2480094	2245	13	0	0	0	0	0
12976	CDS1	10	58	2480094	2245	13	100	0	33	0	0
12977	CDS1	10	58	2480094	2245	13	100	0	25	0	0

ORIGINAL PAGE IS
OF POOR QUALITY

SOUTHERN CALIFORNIA CLOUD/SHADOW MAPPING FROM GOES VS DATA
PROJECT 7D-1460 JET PROPULSION LABORATORY, PASADENA, CALIF

GRID CELL	PHYSIC REGION	PHYSI NUMB	FILE SEQ	SENSOR & DATE	TIME GMT	CELL SQ KM	% AREA CLOUD	% AREA SHADOW	% CLOUD OPAQUE	% SHAD OPAQUE	% BAD DATA
13097	CCS1	10	58	2480094	2245	13	100	0	46	0	0
13098	CCS1	10	58	2480094	2245	13	100	0	46	0	0
13099	CCS1	10	58	2480094	2245	13	100	0	42	0	0
13100	CCS1	10	58	2480094	2245	13	100	0	42	0	0
13101	CCS1	10	58	2480094	2245	13	100	0	42	0	0
13102	CCS1	10	58	2480094	2245	13	100	0	50	0	0
13103	CCS1	10	58	2480094	2245	13	100	0	54	0	0
13104	CCS1	10	58	2480094	2245	13	100	0	46	0	0
13105	CCS1	10	58	2480094	2245	13	100	0	42	0	0
13106	CCS1	10	58	2480094	2245	13	100	0	33	0	0
13107	CCS1	10	58	2480094	2245	13	0	0	0	0	0
13108	CCS1	10	58	2480094	2245	13	0	0	0	0	0
13109	CCS1	10	58	2480094	2245	13	0	0	0	0	0
13110	CCS1	10	58	2480094	2245	13	0	0	0	0	0
13228	CCS1	10	58	2480094	2245	13	100	0	54	0	0
13229	CCS1	10	58	2480094	2245	13	100	0	46	0	0
13230	CCS1	10	58	2480094	2245	13	100	0	50	0	0
13231	CCS1	10	58	2480094	2245	13	100	0	58	0	0
13232	CCS1	10	58	2480094	2245	13	100	0	58	0	0
13233	CCS1	10	58	2480094	2245	13	100	0	54	0	0
13234	CCS1	10	58	2480094	2245	13	100	0	54	0	0
13235	CCS1	10	58	2480094	2245	13	100	0	58	0	0
13236	CCS1	10	58	2480094	2245	13	100	0	75	0	0
13237	CCS1	10	58	2480094	2245	13	100	0	67	0	0
13238	CCS1	10	58	2480094	2245	13	100	0	50	0	0
13239	CCS1	10	58	2480094	2245	13	100	0	54	0	0
13240	CCS1	10	58	2480094	2245	13	100	0	54	0	0
13241	CCS1	10	58	2480094	2245	13	100	0	25	0	0
13242	CCS1	10	58	2480094	2245	13	0	0	0	0	0
13243	CCS1	10	58	2480094	2245	13	100	0	25	0	0
13361	CCS1	10	58	2480094	2245	13	100	0	67	0	0
13362	CCS1	10	58	2480094	2245	13	100	0	63	0	0
13363	CCS1	10	58	2480094	2245	13	100	0	42	0	0
13364	CCS1	10	58	2480094	2245	13	100	0	50	0	0
13365	CCS1	10	58	2480094	2245	13	100	0	67	0	0
13366	CCS1	10	58	2480094	2245	13	100	0	71	0	0
13367	CCS1	10	58	2480094	2245	13	100	0	63	0	0
13368	CCS1	10	58	2480094	2245	13	100	0	50	0	0
13369	CCS1	10	58	2480094	2245	13	100	0	42	0	0
13370	CCS1	10	58	2480094	2245	13	100	0	42	0	0
13371	CCS1	10	58	2480094	2245	13	100	0	38	0	0
13372	CCS1	10	58	2480094	2245	13	100	0	38	0	0
13373	CCS1	10	58	2480094	2245	13	100	0	46	0	0
13374	CCS1	10	58	2480094	2245	13	0	0	0	0	0
13495	CCS1	10	58	2480094	2245	13	100	0	58	0	0
13496	CCS1	10	58	2480094	2245	13	100	0	58	0	0
13497	CCS1	10	58	2480094	2245	13	100	0	50	0	0
13498	CCS1	10	58	2480094	2245	13	100	0	54	0	0

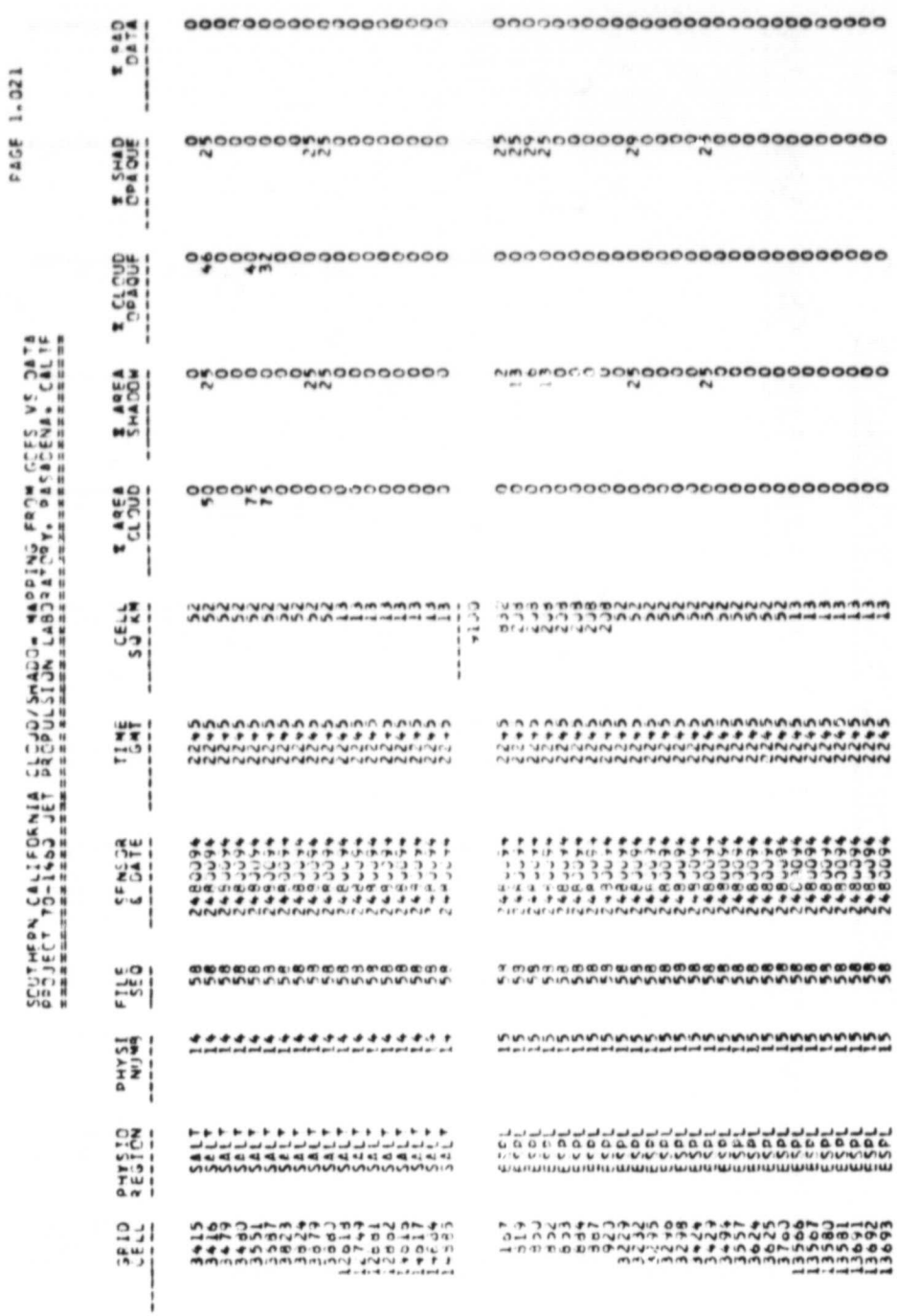

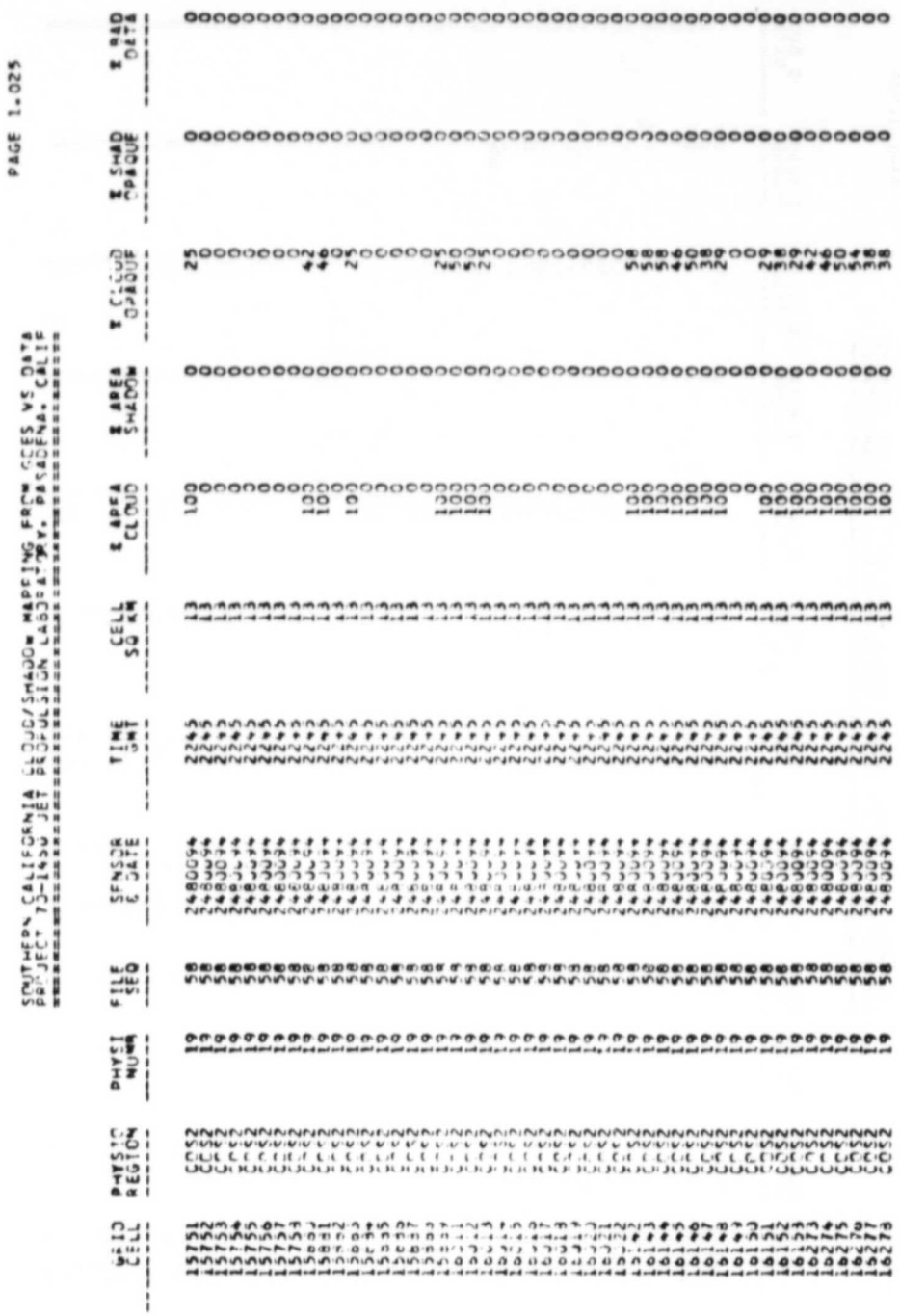

SOUTHERN CALIFORNIA CLOUD/SHADOW MAPPING FROM GOES VS DATA
PROJECT 70-1460 JET PROPULSION LABORATORY, PASADENA, CALIF

GRID CELL	PHYSIO REGION	PHYSI NUMB	FILE SEQ	SENSOR & DATE	TIME GMT	CELL SQ KM	% AREA CLOUD	% AREA SHADOW	% CLOUD OPAQUE	% SHAD OPAQUE	% BAD DATA
16279	COS2	19	58	2480094	2245	13	100	0	25	0	0
16280	COS2	19	58	2480094	2245	13	0	0	0	0	0
16281	COS2	19	58	2480094	2245	13	0	0	0	0	0
16282	COS2	19	58	2480094	2245	13	0	0	0	0	0
16283	COS2	19	58	2480094	2245	13	0	0	0	0	0
16284	COS2	19	58	2480094	2245	13	0	0	0	0	0
16285	COS2	19	58	2480094	2245	13	0	0	0	0	0
16405	COS2	19	58	2480094	2245	13	100	0	58	0	0
16406	COS2	19	58	2480094	2245	13	100	0	54	0	0
16407	COS2	19	58	2480094	2245	13	100	0	46	0	0
16408	COS2	19	58	2480094	2245	13	100	0	54	0	0
16409	COS2	19	58	2480094	2245	13	100	0	50	0	0
16410	COS2	19	58	2480094	2245	13	100	0	50	0	0
16411	COS2	19	58	2480094	2245	13	100	0	29	0	0
16412	COS2	19	58	2480094	2245	13	100	0	25	0	0
16413	COS2	19	58	2480094	2245	13	100	0	33	0	0
16414	COS2	19	58	2480094	2245	13	100	0	29	0	0
16415	COS2	19	58	2480094	2245	13	100	0	38	0	0
16416	COS2	19	58	2480094	2245	13	100	0	33	0	0
16417	COS2	19	58	2480094	2245	13	100	0	25	0	0
16537	COS2	19	58	2480094	2245	13	100	0	50	0	0
16538	COS2	19	58	2480094	2245	13	100	0	50	0	0
16539	COS2	19	58	2480094	2245	13	100	0	42	0	0
16540	COS2	19	58	2480094	2245	13	100	0	42	0	0
16541	COS2	19	58	2480094	2245	13	100	0	42	0	0
16542	COS2	19	58	2480094	2245	13	0	0	0	0	0
16543	COS2	19	58	2480094	2245	13	0	0	0	0	0
16544	COS2	19	58	2480094	2245	13	0	0	0	0	0
16545	COS2	19	58	2480094	2245	13	0	0	0	0	0
16546	COS2	19	58	2480094	2245	13	0	0	0	0	0
16547	COS2	19	58	2480094	2245	13	0	0	0	0	0
16548	COS2	19	58	2480094	2245	13	0	0	0	0	0
16549	COS2	19	58	2480094	2245	13	100	0	25	0	0
16668	COS2	19	58	2480094	2245	13	100	0	58	0	0
16669	COS2	19	58	2480094	2245	13	100	0	63	0	0
16670	COS2	19	58	2480094	2245	13	100	0	63	0	0
16671	COS2	19	58	2480094	2245	13	100	0	58	0	0
16672	COS2	19	58	2480094	2245	13	100	0	63	0	0
16673	COS2	19	58	2480094	2245	13	100	0	58	0	0
16674	COS2	19	58	2480094	2245	13	100	0	29	0	0
16675	COS2	19	58	2480094	2245	13	0	0	0	0	0
16676	COS2	19	58	2480094	2245	13	0	0	0	0	0
16677	COS2	19	58	2480094	2245	13	0	0	0	0	0
16678	COS2	19	58	2480094	2245	13	0	0	0	0	0
16679	COS2	19	58	2480094	2245	13	100	0	33	0	0
16680	COS2	19	58	2480094	2245	13	100	0	46	0	0

ORIGINAL PAGE IS
OF POOR QUALITY

SOUTHERN CALIFORNIA CLOUD/SHADOW MAPPING FROM GOES VS DATA
PROJECT 70-1450 JET PROPULSION LABORATORY, PASADENA, CALIF

GRID CELL	PHYSIO REGION	PHYSI NUMB	FILE SEQ	SENSOR & DATE	TIME GMT	CELL SQ KM	% AREA CLOUD	% AREA SHADOW	% CLOUD OPAQUE	% SHAD OPAQUE	% BAD DATA
						2223					
154	ISL2	20	58	2480094	2245	624	98	0	57	0	0
15139	ISL2	20	58	2480094	2245	13	100	0	42	0	0
15190	ISL2	20	58	2480094	2245	13	0	0	0	0	0
15191	ISL2	20	58	2480094	2245	13	100	0	33	0	0
15320	ISL2	20	58	2480094	2245	13	100	0	50	0	0
15321	ISL2	20	58	2480094	2245	13	100	0	38	0	0
15322	ISL2	20	58	2480094	2245	13	100	0	33	0	0
15323	ISL2	20	58	2480094	2245	13	100	0	33	0	0
15451	ISL2	20	58	2480094	2245	13	100	0	42	0	0
15452	ISL2	20	58	2480094	2245	13	100	0	50	0	0
15453	ISL2	20	58	2480094	2245	13	100	0	50	0	0
15454	ISL2	20	58	2480094	2245	13	100	0	33	0	0
15455	ISL2	20	58	2480094	2245	13	0	0	0	0	0
15456	ISL2	20	58	2480094	2245	13	100	0	29	0	0
15583	ISL2	20	58	2480094	2245	13	100	0	58	0	0
15584	ISL2	20	58	2480094	2245	13	100	0	50	0	0
15585	ISL2	20	58	2480094	2245	13	100	0	63	0	0
15586	ISL2	20	58	2480094	2245	13	100	0	63	0	0
15587	ISL2	20	58	2480094	2245	13	100	0	63	0	0
15717	ISL2	20	58	2480094	2245	13	100	0	38	0	0
15718	ISL2	20	58	2480094	2245	13	100	0	42	0	0
15719	ISL2	20	58	2480094	2245	13	100	0	46	0	0
15720	ISL2	20	58	2480094	2245	13	100	0	50	0	0
15849	ISL2	20	58	2480094	2245	13	100	0	58	0	0
15850	ISL2	20	58	2480094	2245	13	100	0	58	0	0
15851	ISL2	20	58	2480094	2245	13	100	0	58	0	0
						949					
						128730					

ORIGINAL PAGE IS
OF POOR QUALITY

SOUTHERN CALIFORNIA CLOUD/SHADOW MAPPING FROM GOES VS DATA
SUMMARY TOTALS, JPL PROJECT 7J-1460

PHYSIO REGION	PHYSI NUMB	FILE SEQ	SENSOR & DATE	TIME GMT	CELL SQ KM	% AREA CLOUD	% AREA SHADOW	% CLOUD OPAQUE	% SHAD OPAQUE	% BAD DATA
EMJ1	1	59	2480094	2245	41522	2	4	3	12	0
MTN3	2	59	2480094	2245	3123	3	10	1	19	0
MTN1	3	58	2480094	2245	962	0	8	0	13	0
MMJ1	4	59	2480094	2245	14170	3	2	13	11	0
RIVY	5	59	2480094	2245	10562	0	3	4	17	0
MTN4	6	59	2480094	2245	2288	0	4	0	15	0
MTN2	7	59	2480094	2245	16473	18	3	21	7	0
INLA	8	59	2480094	2245	3172	21	0	15	0	0
[illegible]MT1	9	59	2480094	2245	39	67	0	24	0	0
COS1	10	59	2480094	2245	2268	85	0	41	0	0
[illegible]	11	59	2480094	2245	[illegible]	26	1	20	1	0
[illegible]AT2	12	59	2480094	2245	[illegible]	41	1	31	1	0
[illegible]CEN	13	59	2480094	2245	10075	39	0	53	0	0
SBL[illegible]	14	59	2480094	2245	[illegible]	11	5	18	14	0
[illegible]	15	59	2480094	2245	3146	0	3	0	13	0
[illegible]1	16	59	2480094	2245	312	0	4	0	4	0
[illegible]SL1	17	59	2480094	2245	754	90	0	38	0	0
[illegible]2	18	59	2480094	2245	658	3	5	3	5	0
[illegible]S2	19	59	2480094	2245	2223	58	0	25	0	0
ISL2	20	59	2480094	2245	449	96	0	52	0	0
					128700					